

HOSTED BY



Contents lists available at ScienceDirect

Saudi Journal of Biological Sciences

journal homepage: www.sciencedirect.com



Original article

Optimization of subtilisin production from *Bacillus subtilis* strain ZK3 and biological and molecular characterization of synthesized subtilisin capped nanoparticles

Shreya S. Shettar^a, Zabin K. Bagewadi^{a,*}, Harsh N. Kolvekar^a, T.M. Yunus Khan^b,
Shaik Mohamed Shamsudeen^c

^a Department of Biotechnology, KLE Technological University, Hubballi, Karnataka 580031, India

^b Department of Mechanical Engineering, College of Engineering, King Khalid University, Abha 61421, Saudi Arabia

^c Department of Diagnostic Dental Science and Oral Biology, College of Dentistry, King Khalid University, Abha 61421, Saudi Arabia



ARTICLE INFO

Article history:

Received 3 August 2023

Revised 22 August 2023

Accepted 1 September 2023

Available online 6 September 2023

Keywords:

Bacillus subtilis

Subtilisin

Response surface methodology

Nanoparticles

Biological attributes

Analytical characterization

ABSTRACT

The increase and dissemination of multi-drug resistant bacteria have presented a major healthcare challenge, making bacterial infections a significant concern. The present research contributes towards the production of bioactive subtilisin from a marine soil isolate *Bacillus subtilis* strain ZK3. Custard apple seed powder (raw carbon) and mustard oil cake (raw nitrogen) sources showed a pronounced effect on subtilisin production. A 7.67-fold enhancement in the production was evidenced after optimization with central composite design-response surface methodology. Subtilisin capped silver (AgNP) and zinc oxide (ZnONP) nanoparticles were synthesized and characterized by UV-Visible spectroscopy. Subtilisin and its respective nanoparticles revealed significant biological properties such as, antibacterial activity against all tested pathogenic strains with potential against *Escherichia coli* and *Pseudomonas aeruginosa*. Prospective antioxidant behavior of subtilisin, AgNP and ZnONP was evidenced through radical scavenging assays with ABTS and DPPH. Subtilisin, AgNP and ZnONP revealed cytotoxic effect against cancerous breast cell lines MCF-7 with IC₅₀ of 83.48, 3.62 and 7.57 µg/mL respectively. Characterizations of nanoparticles were carried out by Fourier transform infrared spectroscopy, scanning electron microscopy with energy dispersive X-ray, X-ray diffraction, thermogravimetric analysis and atomic force microscopy analysis to elucidate the structure, surface and thermostability properties. The study proposes the potential therapeutic applications of subtilisin and its nanoparticles, a way forward for further exploration in the field of healthcare.

© 2023 The Author(s). Published by Elsevier B.V. on behalf of King Saud University. This is an open access article under the CC BY-NC-ND license (<http://creativecommons.org/licenses/by-nc-nd/4.0/>).

1. Introduction

The prevalence of microbial illnesses has a severe negative impact on human health and has worsened globally due to multi-drug resistant in bacteria (Prabhawathi et al., 2019). Conse-

quently, there is now increased focus on the development of novel antimicrobial agents to address this outbreak. Several bioactive molecules' antimicrobial effects on bacteria have been extensively documented in numerous studies (Vasconcelos et al., 2018). Antibiotic identification has lessened the prevalence of infectious illnesses and saved numerous lives. Nonetheless, the extensive utilization of antibiotics in recent times has resulted in the swift development of multidrug-resistant "superbug" variants, rendering infectious diseases progressively challenging to manage using the current categories of antibiotics. The notion of one health highlights the critical interaction of human, animal, and environmental components in the control of antimicrobial resistance (AMR) which has been rising disproportionately over the past decades. Consequently, there is a pressing necessity to create novel categories of antimicrobial agents (Taneja and Sharma, 2019; Zhou et al., 2019). There appears to be a boost in the number of instances of

* Corresponding author at: Department of Biotechnology, KLE Technological University, Vidyanagar, Hubballi 580 031, India.

E-mail addresses: 01fe21rbt003@kletech.ac.in (S.S. Shettar), zabin@kletech.ac.in (Z.K. Bagewadi), 01fe19bbt006@kletech.ac.in (H.N. Kolvekar), mtatagar@kku.edu.sa (T.M. Yunus Khan), sshahul@kku.edu.sa (S.M. Shamsudeen).

Peer review under responsibility of King Saud University.



Production and hosting by Elsevier

<https://doi.org/10.1016/j.sjbs.2023.103807>

1319-562X/© 2023 The Author(s). Published by Elsevier B.V. on behalf of King Saud University.

This is an open access article under the CC BY-NC-ND license (<http://creativecommons.org/licenses/by-nc-nd/4.0/>).

lifestyle and genetic disorders over the last few decades, like cancers and neurodegenerative disorders, are the conditions characterized by the progressive degeneration of nerve cells (including Parkinson's, Alzheimer's and Huntington's diseases), significantly impacting the quality of life which have given rise to the progress in advanced science and technology in overcoming these challenges (Khandia et al., 2019). Cancer is an illness which triggers abnormal proliferation of cells, which can be either malignant or benign and is said to be the major life-threatening diseases. The global burden of cancer continues to escalate, imposing significant physical, emotional and financial stress on individuals and healthcare systems (Saji et al., 2021). Numerous treatment approaches, including radiation, chemotherapy and surgeries are accessible for combating cancer. Nevertheless, the frequent occurrence of chemotherapy failure is consistently reported and primarily linked to the development of drug-resistant cancer cells. As a result, extensive efforts are being undertaken in the battle against cancer (Alfarouk et al., 2015; Thankappan et al., 2021). Antimicrobial peptides (AMPs) serve as suitable blueprints for an alternative class of potential therapeutics. Among the three major industrial enzyme groups, microbial proteases stand out, representing approximately 65% of the total enzyme sales across the globe. Bacterial subtilisin, primarily derived from *Bacillus subtilis*, constitute a significant group of enzymes. Among these, the subtilisin (EC 3.4.21.14) family, which is generated by diverse *Bacillus* species, is the second-highest domain belonging to the S8 superfamily of serine proteases. In recent studies, patent researches focusing on novel wild-type subtilisin have gained attention. Notably, the patent literature highlights the suitability of subtilisin derived from *Bacillus* sp. for different applications. The ability of thermo-stable halo-alkaline protease to eliminate blood stains, indicated that the protease under investigation had the potential to serve as an additive in detergent formulations in industries (Asitok et al., 2022). Incorporating alkaline serine proteases into procedures such as soaking and dehairing presents a more eco-conscious choice for the leather industry, standing as a greener substitute when compared to conventional techniques. Moreover, crude formulations possessing elastolytic characteristics yield leather of relatively high quality, featuring the desired attributes of strength, suppleness, and texture, all achieved within a shorter timeframe (Matkawala et al., 2021). Conversely, within the realm of microbial fibrinolytic enzymes, subtilisin has garnered significant medical attention in recent years and it is seen as a potential candidate for thrombolytic therapy (Gulmez et al., 2018). The outcomes of the research contribute significantly to the advancement of highly efficient recombinant subtilisin from *Bacillus subtilis*, showcasing enhanced catalytic properties, antibacterial, antioxidant and anticancer attributes. This progress positions subtilisin as an attractive candidate for potential therapeutic applications in healthcare sector which is recently reported (Shettar et al., 2023). In the dairy industry, enzymes such as proteases are employed in cheese manufacturing. Their fundamental role involves breaking down peptide bonds to produce macro peptides in conjunction with casein. It also has the ability to modify the flavours used in food sector (Naveed et al., 2021). Various *Bacillus* species produce a number of popular nattokinase/subtilisin enzymes such as, *Bacillus subtilis*, *Bacillus licheniformis*, *Bacillus amylosacchariticus* and *Bacillus amyloliquefaciens* (Modi et al., 2023). Ever since the first identification of subtilisin Carlsberg, an alkaline protease derived from *B. licheniformis* is widely used in the detergent industry. Numerous alkaline proteases from various sources like *B. circulans* DZ100 (Benkiar et al., 2013), *Geobacillustoebii* Strain LBT 77 (Thebti et al., 2016), *Aeribacillus pallidus* (Mechri et al., 2017; Yildirim et al., 2017), *B. lentus*, *B. clausii* and *B. alkalophilus* (Azrin et al., 2022) etc. have been thoroughly studied and investigated for an array of biotechnological uses. (Salwan and Sharma, 2019). The temperature resistance of

subtilisin from *Bacillus* sp. has been thoroughly investigated, renowned for its ability to withstand heat owing to their characteristics as spore-forming microorganisms. They are mostly active at neutral-mildly alkali pH (Azrin et al., 2022). Creating an ideal medium is critical for increasing output and lowering expenses for production, especially in terms of comprehending the significance and remedial implications of the nattokinase protein as previously described (Modi et al., 2023). A broad spectrum of agricultural leftovers (such as wheat bran, rice bran, gram husk, and sugarcane bagasse) and waste from industries (including oil cakes, whey, and coffee pulp) are employed as suitable substrates for enzyme production. Not only do these residues assist microbial cell proliferation, but they also act as a nutrient reservoir, delivering essential elements for their development (Matkawala et al., 2021, 2019). Subtilisin can be harnessed to disintegrate proteinaceous and stubborn biowastes of frozen fish encountered in ecology and the biowastes are transformed into valuable products such as protein hydrolysates and chitinous materials, which find applications in various other industries (Azrin et al., 2022). Utilizing agro-food residue and in situ enzyme synthesis as part of a biorefining technique, when compared to present industrial techniques that entail hefty substrates, the operational expenses of the bioprocess could be significantly lowered. This approach not only helps in reducing waste disposal problems but also creates a sustainable and cost-effective solution for enzyme production. Additionally, it contributes to the overall goal of promoting a circular economy and minimizing the environmental impact of agro-waste (Sharma et al., 2022). Emerging research on nanoparticles have garnered significant interest due to their extensive utilization across diverse industries, including agriculture, medicines, consumer goods, power, transportation, skincare products, and, perhaps most significantly, as antimicrobial compounds (Li et al., 2017). Factors such as metal ion concentration, temperature, concentration, reaction time and solvent type play an indispensable part in defining the antimicrobial capabilities of nanoparticles (Mba and Nweze, 2021).

Nevertheless, not many studies have been reported on the production of subtilisin using *B. subtilis* strain with insights on its nanoparticle behavior and its biological activities. In the current study, subtilisin production using agro-wastes was executed and to enhance its yield statistical optimization employing central composite design-response surface methodology (CCD-RSM) was carried out that revealed a 7.67-fold enhancement of subtilisin. Subtilisin-capped silver and zinc oxide nanoparticles were synthesized and assessed for biological activities like antibacterial, antioxidant and anticancer. The capped-nanoparticles were studied for its structural behavior using various analytical techniques like Fourier transform infrared spectroscopy (FTIR), Scanning electron microscopy (SEM) with energy dispersive X-ray Spectroscopy (EDS) analysis, Thermogravimetric analysis (TGA), Atomic Force Microscopy (AFM) and X-Ray Diffraction (XRD). The present study has brought forward remarkable and impressive biological activities and nanoparticle behaviour with subtilisin prompting it to explore its potentiality in applications of healthcare.

2. Materials and methods

2.1. Chemicals and microbial cultures

The components that were utilized in this present investigation were: purchased from Merck and Co. Inc. (USA) and Sigma-Aldrich Pvt Ltd. (USA). Raw agricultural waste was procured from locally available industries. The pathogenic strains utilized in the antibacterial studies, including *Pseudomonas aeruginosa* (MTCC 2297), *Salmonella typhimurium* (MTCC 98), *Bacillus licheniformis* (MTCC 429 T), *Bacillus cereus* (NCIM 2217), *Escherichia coli* (MTCC 443)

and *Staphylococcus aureus* (MTCC 737) were obtained from the National Collection of Industrial Microorganisms (NCIM), Pune and Microbial Type Culture Collection and Gene Bank (MTCC), Chandigarh. Anticancer studies were conducted using breast cancer MCF-7 cell lines.

2.2. Isolation, screening and gene sequencing of subtilisin producer

As subtilisin falls within the serine protease family, initially protease producing bacterial culture was isolated from marine soil collected from Karwar regions, Karnataka, India. Serial dilution and plating on casein supplemented nutrient agar medium supplemented with (g/L) peptone 5; yeast extract 1.5; Nalco 5; beef extract 1.5; casein 10 and agar 20 (pH 9.0) were used to isolate the bacterial strain. To generate distinguished bacterial colonies, plates were left to incubate at 35 ± 2 °C. The cultures showing clear halo were regarded as positive for protease production and purified by sequential streaking. The prominent pure cultures were subsequently examined and further screened on a skim milk agar plate having (g/L) skim milk 20; glucose 10 and agar 20 (pH 9.0) followed by incubation at 35 ± 2 °C to obtain clear zones. The ratio of clear zone was calculated (Alahdal et al., 2022; Hakim et al., 2018) and the potential strain showing highest zone was selected as protease producer for the present study. The single culture had been kept at 4 °C on a nutrient agar slant with frequent sub-culturing. The strain ZK3 that was isolated was discovered using previously established techniques of 16S rRNA gene sequencing (Bagewadi et al., 2020a). In a concise manner, genomic DNA was extracted from the selected culture and amplified using primers specific to the 16S rRNA gene, namely, 704F and 907R employing Veriti® 96-well Thermal Cycler (Model No. 9902 Applied Biosystems, USA) to obtain an identifiable polymerase chain reaction (PCR) amplicon band. The details of the PCR reaction is summarized in the previous report (Bagewadi et al., 2022). Post purification of PCR product, it underwent sequencing using BDT v3.1 Cycle Sequencing Kit on ABI 3730xl Genetic Analyser, Applied Biosystems, USA. The sequences were aligned and analyzed for similarity by using the NCBI (National Center for biotechnology information) BLAST tool and ClustalW multiple aligner. RDP (the Ribosomal Database Project) database (<https://rdp.cme.msu.edu>) was adopted to create a distance matrix. MEGA 11 software was used to generate the phylogenetic tree using the neighbor-joining approach to find the closest affiliated strains (Bagewadi et al., 2020b).

2.3. Subtilisin production from isolated bacterial culture

The potential protease producer ZK3 strain was employed for production of subtilisin. Strain ZK3 inoculum was prepared by transferring a culture loop in 50 mL nutrient broth (pH 9.0) supplemented with 1% casein followed by 24 h incubation at 35 ± 2 °C at 200 rpm in a rotating shaker (Scigenic biotech, India). A 5% inoculum had been dissolved into 100 mL of subtilisin production medium containing (g/L) casein 10; NH₄Cl 1; NaCl 1; KH₂PO₄ 0.8; K₂HPO₄ 0.6; MgSO₄ 0.5 and yeast extract 0.2 (pH 9.0) in 250 mL Erlenmeyer flask (Abdullah Al-Dhabi et al., 2020; Asitok et al., 2022; Wehaidy et al., 2020). The flask was incubated for 5 days (35 °C, 200 rpm). Samples (bacterial culture) were harvested at a regular period of every 24 h. To remove cell debris, the samples were spun down for a duration of 10 min at 10,000 revolutions (rpm) (4 °C), and the resulting liquid which is called as supernatant, served as the source of subtilisin for the experiment.

2.4. Analytical measurements

2.4.1. Subtilisin activity

Subtilisin activity was measured using the synthetic peptide (N-Suc-F-A-A-F-pNA) (catalog number S2628, Sigma Aldrich). The reaction was set up by incubating a mixture (200 µL) consisting of enzyme solution (30 µL), synthetic (chromogenic) peptide (30 µL), and 20 mM Tris-HCl (pH 7.4) (140 µL) for 30 min at 37 °C. UV-Visible spectrophotometry at 405 nm was used for evaluating the quantity of emitted *p*-nitroaniline. Under standard assay conditions, the quantity of enzyme releasing 1 µmol of *p*-NA per minute defines one unit of enzymatic activity on a synthetic peptide. (Couto et al., 2022; Mechri et al., 2022).

2.4.2. Determination of protein content

BCA protein assay kit was used to assess the overall soluble protein concentration (mg) of subtilisin (Bagewadi et al., 2017a) with standard bovine serum albumin. In triplicate, measurements were taken, and the results were reported as mean \pm standard deviation.

2.5. Optimization of subtilisin by OFAT

2.5.1. Effect of raw carbon sources on subtilisin production

Carbon sources are believed to have a substantial influence on growth, enzyme production and metabolism of bacteria. Several raw carbon sources such as, molasses (M), wheat bran (WB), sweet sorghum bagasse (SSB) and custard apple seed powder (CASP) (1% w/v) were evaluated for the production of subtilisin (U/mL). Sweet sorghum stalks were collected, washed and processed to remove the juice. The obtained bagasse was dried and powdered to obtain SSB. Similarly, custard apple seeds were collected washed, dried and powdered to get CASP, M, WB, SSB and CASP (1% w/v) were supplemented in the subtilisin production medium as described above containing glucose (1% w/v). Production medium containing glucose (1% w/v) served as control. For three days, the production was processed at 35 °C and 200 rpm. All investigations were performed in triplicates in a monitored environment. The collected samples were examined to determine subtilisin activity (U/mL) as described above.

2.5.2. Effect of raw nitrogen sources on subtilisin production

In the preliminary study, a one-factor optimization method was utilized to test various nitrogen sources. To find out how different nitrogen sources affect subtilisin synthesis, agricultural waste materials such as oil cakes of groundnut, mustard and safflower were available locally, and incorporated in production media as described above containing glucose (1% w/v). Production medium containing 1% glucose was served as control. The production was conducted with incubation at 35 °C and 200 rpm for a duration of 3 days. All the experiments were performed in triplicates in a controlled setting. As described above, samples were harvested and analyzed for subtilisin activity (U/mL) (Elumalai et al., 2020).

2.6. Plackett-Burman design (PBD) analysis of key variables influencing subtilisin production

The significant factors affecting subtilisin production were screened using Plackett-Burman Design (PBD). Drawing on the initial assessment of raw carbon and nitrogen sources, a PBD of 12 experimental runs was designed using Minitab 17 statistical software. Experiments constituted at two different levels: high (+1) as well as low (-1) for all the 10 variables namely, casein (X₁), NH₄Cl (X₂), NaCl (X₃), KH₂PO₄ (X₄), K₂HPO₄ (X₅), MgSO₄ (X₆), yeast extract (X₇), glucose (X₈), mustard oil cake (X₉) and CASP (X₁₀). Experiments were set at pH 9 and 35 °C for 3 days in triplicates.

The PBD matrix, encompassing actual and coded values of variables along with respective experimental responses are indicative in Table 1. The yield (response) demonstrates the average subtilisin production (U/mL). *Y* denotes the outcome of the experiment response, which was derived from the first-order polynomial model equation (Bagewadi et al., 2018).

2.7. Subtilisin optimization by response surface methodology (RSM)

Based on the findings of PBD, five levels ($-\alpha$, -1 , 0 , $+1$ and $+\alpha$) CCD of response surface methodology (RSM) was employed for optimization of four significant factors namely, glucose (A), mustard oil cake (B), CASP (C) and casein (D) using Minitab 17 statistical software. The experimental process parameters were set at pH 9, 35 °C for 3 days. For the relevant factors, five levels were established, and other medium components were believed to be constant. Each experimental run was executed in replicates. The CCD-RSM design matrix with mean results (subtilisin yield U/mL) represented as *Y* are depicted in Table 3. The relationship among the coded and actual values of variables is derived from the previously reported equation (Bagewadi et al., 2017b). The mean response was resultant from the second-order polynomial quadratic Eq. (1) as represented below:

$$Y = \beta_0 + \beta_1A + \beta_2B + \beta_{11}A^2 + \beta_{22}B^2 + \beta_{12}AB \quad (1)$$

Here, *Y* depicts the calculated average response, β_0 is the model's intercept, β_1 and β_2 are linear term coefficients, β_{11} and β_{22} are coefficients for second-order terms and β_{12} is the coefficient of interactions among A and B.

Furthermore, the three-dimensional interaction surface plots show how the factors interact with one another. The analysis of variance, also known as ANOVA, determines the importance of the model variables and their relationship with the anticipated response. The Fisher's 'F' value and probability 'p' are used to calculate the model's significance and the accuracy of the model is indicative from the coefficient of determination R^2 and adjusted R^2 . Following the experimentation, the developed model was validated furthering replicates with optimized variable conditions and other process parameters were set at pH 9, 35 °C for 3 days as mentioned above.

Table 1
Plackett-Burman design matrix for evaluating important elements influencing subtilisin production.

Run No.	X ₁ Casein (%)	X ₂ NH ₄ Cl (%)	X ₃ NaCl (%)	X ₄ KH ₂ PO ₄ (%)	X ₅ K ₂ HPO ₄ (%)	X ₆ MgSO ₄ (%)	X ₇ Yeast extract (%)	X ₈ Glucose (%)	X ₉ Mustard oil cake (%)	X ₁₀ CASP (%)	Subtilisin production yield (U/mL)	
											Experimental	Predicted
1	(+1)3	(-1)0.1	(+1)0.3	(-1)0.08	(-1)0.06	(-1)0.05	(+1)0.06	(+1)3	(+1)3	(-1)1	39.5090 ± 0.8	39.6471
2	(+1)3	(+1)0.3	(-1)0.1	(+1)0.24	(-1)0.06	(-1)0.05	(-1)0.02	(+1)3	(+1)3	(+1)3	55.0100 ± 0.6	54.8719
3	(-1)1	(+1)0.3	(+1)0.3	(-1)0.08	(+1)0.18	(-1)0.05	(-1)0.02	(-1)1	(+1)3	(+1)3	36.7000 ± 1.2	36.8381
4	(+1)3	(-1)0.1	(+1)0.3	(+1)0.24	(-1)0.06	(+1)0.15	(-1)0.02	(-1)1	(-1)1	(+1)3	34.0740 ± 1.0	34.2121
5	(+1)3	(+1)0.3	(-1)0.1	(+1)0.24	(+1)0.18	(-1)0.05	(+1)0.06	(-1)1	(-1)1	(-1)1	27.9890 ± 0.5	28.1271
6	(+1)3	(+1)0.3	(+1)0.3	(-1)0.08	(+1)0.18	(+1)0.15	(-1)0.02	(+1)3	(-1)1	(-1)1	33.6120 ± 0.2	33.4739
7	(-1)1	(+1)0.3	(+1)0.3	(+1)0.24	(-1)0.06	(+1)0.15	(+1)0.06	(-1)1	(+1)3	(-1)1	28.0471 ± 0.7	27.9090
8	(-1)1	(-1)0.1	(+1)0.3	(+1)0.24	(+1)0.18	(-1)0.05	(+1)0.06	(+1)3	(-1)1	(+1)3	35.7100 ± 1.4	35.5719
9	(-1)1	(-1)0.1	(-1)0.1	(+1)0.24	(+1)0.18	(+1)0.15	(-1)0.02	(+1)3	(+1)3	(-1)1	38.0099 ± 0.4	38.1480
10	(+1)3	(-1)0.1	(-1)0.1	(-1)0.08	(+1)0.18	(+1)0.15	(+1)0.06	(-1)1	(+1)3	(+1)3	35.9000 ± 1.5	35.7619
11	(-1)1	(+1)0.3	(-1)0.1	(-1)0.08	(-1)0.06	(+1)0.15	(+1)0.06	(+1)3	(-1)1	(+1)3	32.3000 ± 0.9	32.4381
12	(-1)1	(-1)0.1	(-1)0.1	(-1)0.08	(-1)0.06	(-1)0.05	(-1)0.02	(-1)1	(-1)1	(-1)1	21.9600 ± 1.3	21.8219

The mean ± standard deviation of triplicates is employed to represent each experimental value. CASP = Custard Apple Seed Powder.

2.8. Production kinetics of subtilisin

The designed optimized media conditions were employed for the analysis of subtilisin production kinetics over a period of 4 days. Independent production flasks were set up while samples were collected at 24-hour intervals for assessment. Subtilisin production (U/mL), cell biomass (OD at 660 nm), protein (mg) and residual substrate (reducing sugar) (mg/mL) were estimated. The reducing sugar content in the fermentation mixture was determined using the DNS (Dinitrosalicylic acid) technique by Bagewadi et al. (2016). In a nutshell, 1.0 mL of sample was spun (10,000 rpm, 15 min, 4 °C) and 2.0 mL of DNS solution was then supplemented. The reaction was performed in a controlled boiling water bath at 100 °C. An UV-Visible spectrophotometer was utilized to measure the colored product at 540 nm. D-glucose was used as standard, all the estimation were performed in triplicates, and data is represented as mean ± SD.

2.9. Synthesis of subtilisin capped silver and zinc oxide nanoparticles

Subtilisin capped silver nanoparticles (AgNP) were synthesis according to method described by Sidhu and Nehra (2021). Briefly, 5 mM, 10 mM and 50 mM solution of silver nitrate was prepared with constant stirring on magnetic stirrer. Subtilisin (0.5 mL) and silver nitrate (4.5 mL) were incorporated and incubated at ambient temperature for 30 min while exposed to UV radiation followed by microwave heating for 30 sec. UV-Vis Spectroscopy was used to determine the wavelength of AgNP solution. Collected AgNP were separated by spinning at 10,000 revolutions per minute for ten minutes and dried for further characterization.

Zinc oxide nanoparticles (ZnONP) were synthesised with subtilisin by following reaction consisting of 10 mM 700 µL of zinc acetate dehydrate mixed with 300 µL of subtilisin and reaction was incubated at 55 °C for 15 min followed by incubation at ambient temperature for 4 h. UV-Vis spectrophotometric measurements were recorded for a period of 24 h to determine the characteristic spectrum of ZnONP. The obtained precipitate was spun down at 10,000 rpm for 10 min. The recovered precipitate was air-dried in a hot air oven at 50 °C until 24 h and kept for subsequent analysis (Alahdal et al., 2022). The subtilisin capped AgNP and ZnONP synthesized with subtilisin were evaluated for biological properties.

2.10. Functional characterization of subtilisin capped silver and zinc oxide nanoparticles

2.10.1. Antibacterial activity and minimum inhibitory concentration (MIC)

The antibacterial capability of subtilisin and subtilisin capped AgNP and ZnONP was investigated by agar-well diffusion technique against Gram positive (*S. aureus*, *B. licheniformis* and *B. cereus*) and Gram negative (*Escherichia coli*, *Salmonella typhimurium* and *P. aeruginosa*) pathogens. These pathogen cultures were prepared in Luria broth (LB) media and treated overnight (37 °C). Using Luria agar (LA) plates, the turbid culture mixture was inoculated. Wells were created with sterile cork borer (6 mm) and 100 µL of respective samples (subtilisin, subtilisin capped AgNP and ZnONP) were loaded in the wells and subjected for diffusion at 4 °C (2 h). After incubating the plates overnight at 37 °C, the measurement of the width of the region of inhibition which extends transverse surrounding the wells was determined. Positive control was cefixime (5 µg/mL). (Bagewadi et al., 2019).

The MIC of subtilisin and subtilisin capped AgNP (50 mM) and ZnONP (50 mM) was carried out using the microbroth dilution technique in compliance with the Clinical and Laboratory Standards Institute (CLSI) standards. The pathogenic cultures were prepared in Mueller-Hinton broth and grown overnight (37 °C) under shaking conditions (150 rpm) to obtain exponential growth phase. The cultures were diluted to attain the desired cell concentration (10⁷ CFU/mL). Concentrations of the indicated sample subtilisin (150, 75, 37.5, 18.75, 9.375 and 4.687 µg/mL) and subtilisin capped AgNP and ZnONP in (50, 25, 12.5, 6.25, 3.125, 1.56 mM) concentrations were prepared in sterilized deionized water. Sample concentrations were introduced to culture broths and cultured for 24 h at 37 °C. The inhibitory effect of subtilisin and subtilisin capped AgNP and ZnONP on the pathogens was assessed by measuring the absorbance (600 nm) spectrophotometrically. Negative control represents un-inoculated broths and positive control represents culture broth without addition of samples. MIC (µg/mL) refers to the lowest concentration where no apparent growth was observed (Amiri et al., 2022; Shettar et al., 2023).

2.10.2. Antioxidant activity

2.10.2.1. α , α -Diphenyl- β -picryl-hydroxyl (DPPH) radical scavenging assay. The DPPH radical scavenging assays of subtilisin, subtilisin capped AgNP (50 mM), and ZnONP (50 mM) were conducted using the technique followed by Manikandan et al. (2021). Briefly, a reaction of 1 mL of respective sample (subtilisin and subtilisin capped AgNP and ZnONP) in a concentration range of 20–200 µg/mL and 1 mL of DPPH (0.135 mM) was incubated (25 °C) under dark conditions for 30 min. The absorbed wavelength of the chemical reaction was measured at 517 nm using UV–Vis spectrophotometer. The scavenging activity percentage was calculated (Manikandan et al., 2021) and ascorbic acid (1 mM) was used as standard.

2.10.2.2. 2,2-azino-bis-3-ethylenebenzothiazoline-6-sulfonic acid (ABTS) assay. The ABTS scavenging activity of subtilisin and subtilisin capped AgNP (50 mM) and ZnONP (50 mM) was conducted with the technique reported previously (Bagewadi et al., 2019). ABTS and potassium persulfate were reacted for 16 h under dark condition to obtain an absorbance of 0.70 at 734 nm. 0.5 mL respective samples were mixed with 2 mL of ABTS solution, resulting in a total volume of 2.5 mL (subtilisin and subtilisin capped AgNP and ZnONP) followed by incubation at 25 °C for 30 min. The reaction's absorbance was measured at 734 nm. The scavenging ability of respective samples (subtilisin and subtilisin capped AgNP and ZnONP) in range of 12–60 h of time period was calculated (Ashokbhai et al., 2022). Butylated hydroxytoluene (BHT) was employed as standard.

2.10.3. Anticancer activity assessment using 3-(4, 5-dimethylthiazol-2-yl) – 2,5-diphenyltetrazolium bromide (MTT) assay

The MTT procedure was carried out to assess the impact of subtilisin and subtilisin capped AgNP and ZnONP on the viability of breast cancer cell line MCF-7 *in-vitro*. To do this, 5000 cells/well of the cancer cells were planted in a 96-well microplate and were incubated for 24 h. To treat the cells, various doses of subtilisin and subtilisin capped AgNP and ZnONP were utilized, for 48 h, with the range of concentrations being from 6.25 to 200 µg/mL. The medium was withdrawn after the treatment, and the cells underwent washing with phosphate-buffered saline (PBS). The cells were then treated for 4 h with MTT (0.5 mg/mL) added to each well. Dimethyl sulfoxide (DMSO) was used to dissipate the formed formazan crystals, and the wavelength of absorption at 570 nm was measured using a microplate reader (BioTek Epoch 2 microplate spectrophotometer). The cells that received no exposure to the aforementioned substances were termed the control group, as they had 100% cell viability. Connecting the absorbance of the treated cells, evaluated their cell survival. Doxorubicin was used as the standard drug. All treatments were conducted in triplicate (Thankappan et al., 2021).

2.11. Analytical characterization of subtilisin-capped silver and zinc oxide nanoparticles

2.11.1. Fourier transform infrared spectroscopy (FTIR) analysis of subtilisin capped nanoparticles

To examine the capping agents present on the surface of subtilisin capped AgNP and ZnONP through FTIR inspection, the samples were grounded into powder. The FTIR examination of the dried and grounded powder was performed using FTIR Spectrometer Nicolet, 5700 instrument using potassium bromide (KBr) pellet method, which operated under the following conditions: a spectral range of 4000–400 cm⁻¹, and a resolution of 1.0 cm⁻¹ (Bagewadi et al., 2020b; Manikandan et al., 2021).

2.11.2. Scanning electron microscopy (SEM) with energy dispersive X-ray (EDS) analysis of subtilisin capped nanoparticles

To study the shape and physical properties of the subtilisin capped AgNP and ZnONP, a Scanning Electron Microscope (SEM) coupled with Energy Dispersive X-ray spectroscopy (EDS) (JEOL make, JSM-IT500L) was utilized. SEM examination was performed on an individual drop of the sample, and the elemental composition of the sample was assessed using an EDS (Bagewadi et al., 2020a; Jeyabharathi et al., 2022; Özbek and Ünal, 2017).

2.11.3. Thermogravimetric analysis (TGA) of subtilisin capped nanoparticles

To assess the thermostability of the subtilisin capped AgNP and ZnONP, TGA analysis was performed using a SDT-Q600 instrument. The powdered nanoparticle sample was subjected to heating in a nitrogen-controlled environment, with a thermal rate of 10 °C/min, in the temperature that varied between 25 and 800 °C (Bagewadi et al., 2020b; Özbek and Ünal, 2017).

2.11.4. Atomic force microscopy (AFM) analysis of subtilisin capped nanoparticles

The particle topography of subtilisin capped AgNP and ZnONP were visualized with an Atomic Force Microscope (AFM) (Nanosurf, Switzerland). A 10 µL drop of nanoparticles was spotted on a glass slide and a thin film was smeared. This was allowed to air dry for few minutes. A piezoelectric scanner was used to mount the sample, which was then scanned using a silicon nitride cantilever in contact mode to examine its surface. The micrographs were interpreted using Easyscan 2 software (Guilger-Casagrande et al., 2021; Prabhawathi et al., 2019).

2.11.5. X-ray diffraction analysis of subtilisin capped nanoparticles

X-ray Diffraction was utilized to investigate the crystallographic properties of subtilisin-capped nanoparticles using the Smart Lab SE in the 2θ range of $20\text{--}90^\circ$ at 40 kV and current of 30 mA with Cu K α radiation (Alahdal et al., 2022; Sidhu and Nehra, 2021).

2.12. Statistical analysis

All tests and activities were executed in triple quantities, and the values are presented in the form of mean \pm standard deviation (SD). The bars displaying errors in each figure indicate the standard deviation (SD), which was determined in Excel, a spreadsheet program.

3. Results

3.1. Screening and molecular characterization of subtilisin producer

The current study reveals isolation of a novel bacterial strain from marine soil from Karwar region, Karnataka, India. The potential isolate ZK3 was isolated using serial dilution technique with 0.9% saline followed by spread plate method on nutrient agar plates. The isolated colony was picked and inoculated into nutrient broth followed by incubation for 24 h at 37 °C. Post incubation, the culture was checked for purity by Gram's stain method to be identified as Gram-positive bacteria with rod shaped morphology. The pure isolate was tested predominantly on casein agar plate showing highest inhibition zone which proves to be capable of producing proteolytic activity. The zone of hydrolysis around the colony depicted the hydrolysis activity of casein as depicted in Fig. S1 in SI. The potential pure variant ZK3 underwent molecular analysis using 16S rRNA gene sequencing and was determined by building

an evolutionary tree using MEGA software v11. Fig. 1 represents the evolutionary structure of the newly discovered isolate of bacteria ZK3, alongside the most closely related analogous sequences. The designated strain was titled *Bacillus subtilis* strain ZK3 16S ribosomal RNA gene partial sequence. The strain's genetic sequence with 1513 bp has been entered into the NCBI database with a specific accession number OQ300503.1. The strain exhibited a significant resemblance to other highly homologous species of *B. subtilis*, as evidenced by its placement on the same branch within the phylogenetic tree.

3.2. Subtilisin production and influence of raw carbon and nitrogen sources

The synthesis of subtilisin (U/mL) was investigated from isolated *B. subtilis* strain ZK3 employing the standard casein production medium (control). The production was evaluated for 5 days (data not shown) and maximum subtilisin production of 9.5 U/mL (control) (Fig. 2A) was obtained on 3rd day with protein content of 0.12 mg/mL. It is commonly acknowledged that microorganisms typically flourish in solutions with isotonic properties. The findings indicated a moderately saline (NaCl) environment could significantly aid in the production of subtilisin. It has been documented that organic nitrogen sources like yeast extract also encompass a carbon element. This carbon presence notably fosters cell growth and the production of polysaccharides (Kumari et al., 2023). Magnesium is a vital element for the growth and division of bacterial cells (Wehaidy et al., 2020) while the utilization of ammonium chloride as an inorganic nitrogen source hinders the production of proteinase (Rozanov et al., 2021). Different types of raw carbon sources (M, WB, SSB and CASP) were assessed for their effect on the subtilisin production. Pronounced effect of CASP was

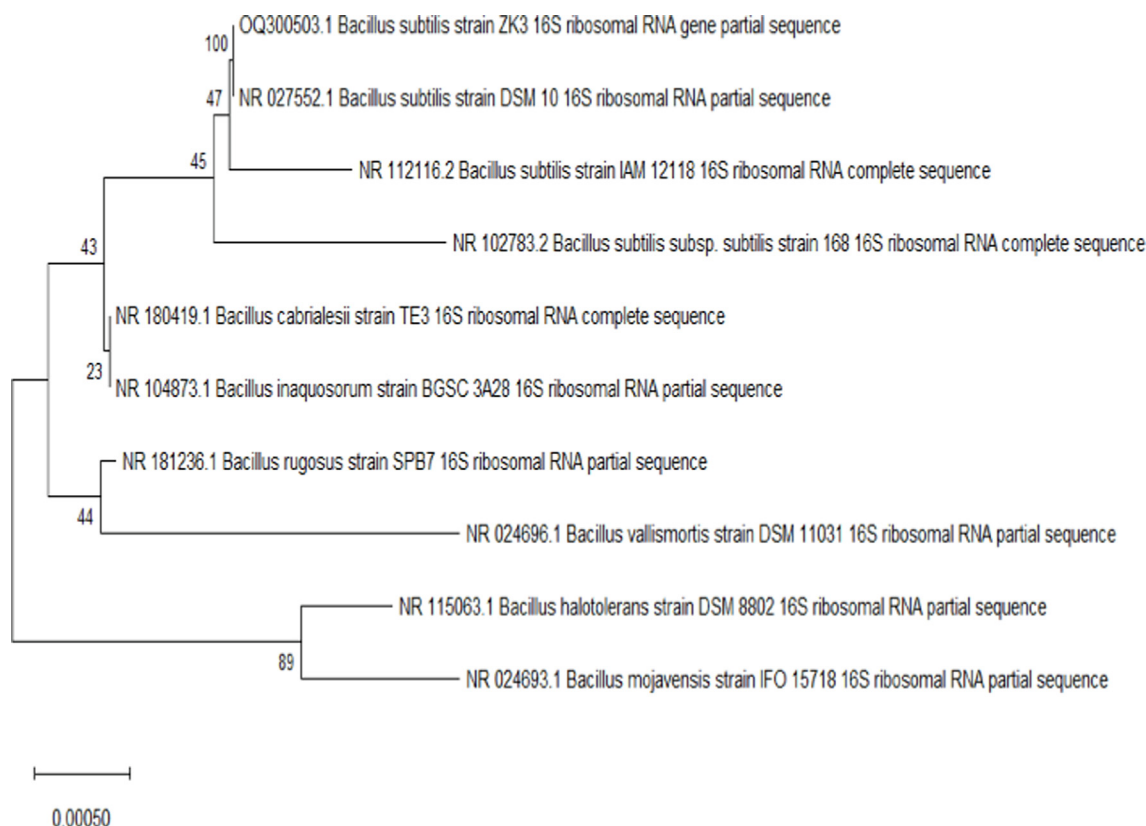


Fig. 1. Phylogenetic tree using neighbor-joining method depicting the position of strain ZK3 (*B. subtilis* strain ZK3 16S ribosomal gene partial sequence; Accession number: OQ300503.1) based on 16 s rRNA sequence and accession in the braces, with sequences from NCBI.

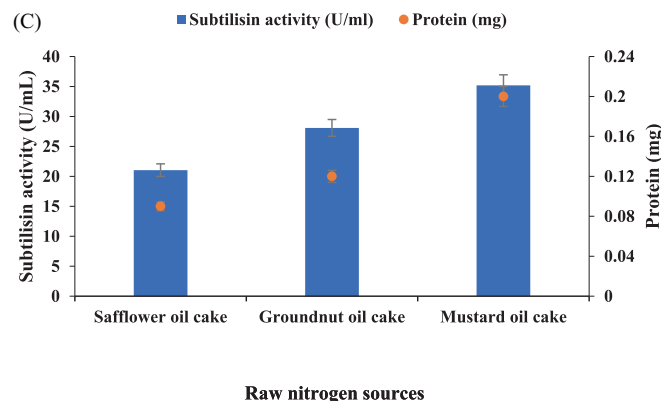
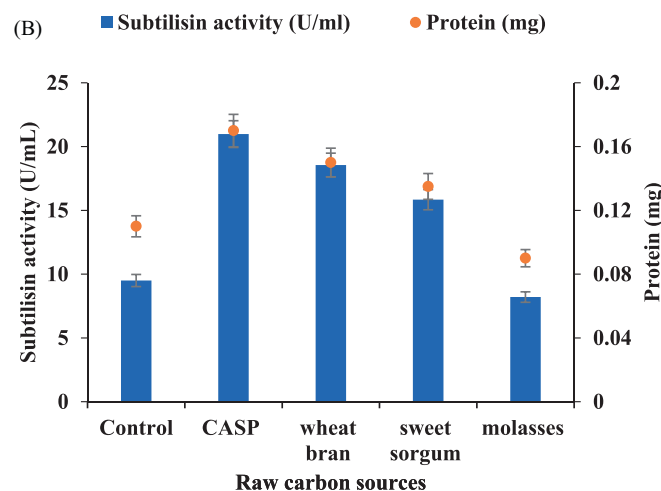
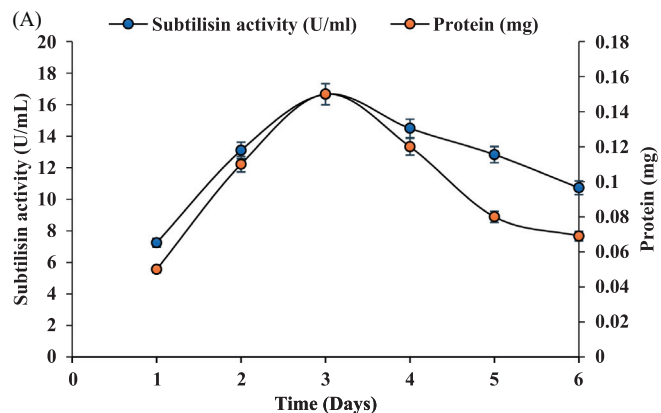


Fig. 2. Production and statistical optimization of subtilisin. Production of subtilisin from *B. subtilis* strain ZK3 (A), Effect of raw carbon source on subtilisin production. Data values reflect triplicate means, whereas the error bars indicate standard deviation (B), Effect of raw nitrogen source on subtilisin production. Data values reflect triplicate means, whereas the error bars indicate standard deviation (C), 3D response surface plot revealing the interaction among glucose vs. CASP (D), glucose vs. casein (E), mustard oil cake vs. casein (F), CASP vs. casein (G), affecting the subtilisin production (U/mL). Results represent a significant interaction with $p < 0.05$, Production kinetics of subtilisin production from *Bacillus subtilis* strain ZK3 (H).

evidenced with 20.97 U/mL and 0.17 mg/mL of protein (Fig. 2B) followed by WB that showed 18.55 U/mL and 0.15 mg/mL of protein. Except of molasses (8.2 U/mL), all the tested raw carbon had the capability to induced subtilisin production. Moreover, with CASP identified as the best and optimal carbon source, investigations

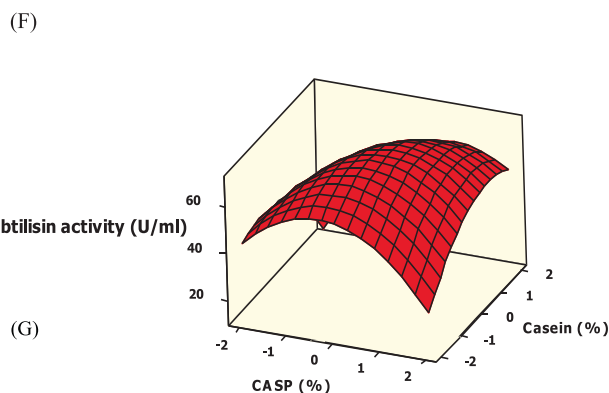
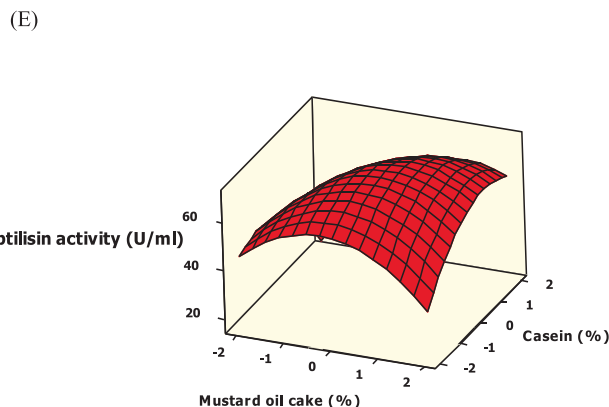
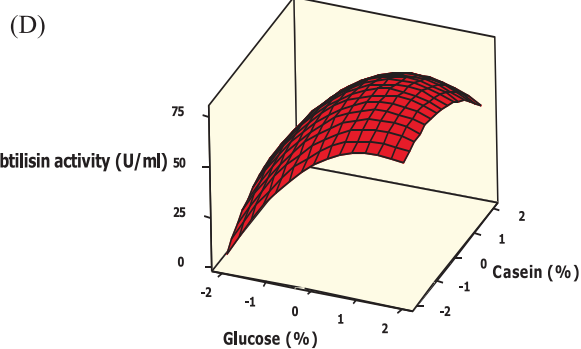
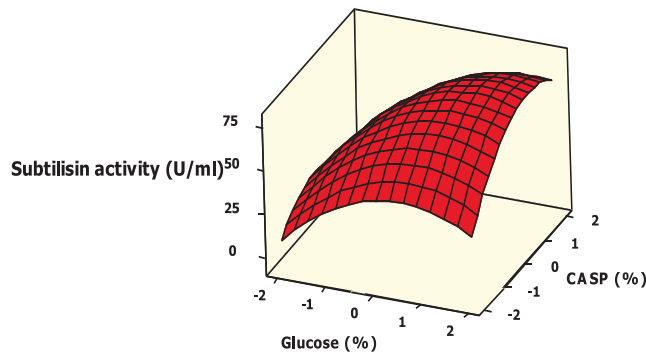
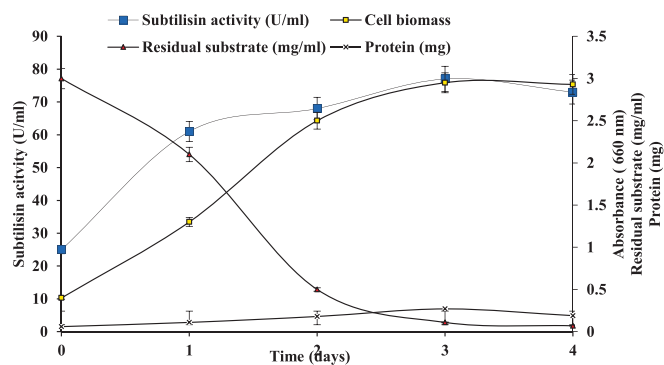


Fig. 2 (continued)

were conducted to explore the impact of different nitrogen sources on subtilisin production. Carbon movement is controlled by both the lipogenic pathway (related to the lipid component) and the glycolytic pathway (related to the hydrophilic component). Both



(H)

Fig. 2 (continued)

of these pathways are restricted by the metabolic processes of microorganisms (Kumari et al., 2023). Amongst all three raw nitrogen sources evaluated (oil cakes of groundnut, mustard and safflower), mustard oil cake generated the most subtilisin of 35.18 U/mL and 0.20 mg/mL of protein (Fig. 2C) followed by groundnut oil cake (28.08 U/mL) that also showed better effect. Safflower oil cake did not produce any much significant effect.

3.3. Investigation of significant factors influencing subtilisin production by PBD

The variables involved in the production of subtilisin by *B. subtilis* strain ZK3 were screening using PBD. The measured and anticipated yields (subtilisin production U/mL) of 12 experimental runs as responses are displayed in Table 1. Run no. 2 in the designed matrix reflects maximum production of 55 U/mL with casein, CASP, mustard oil cake, glucose, NH₄Cl and KH₂PO₄ present at high level (+1). The variability in the yields ranging from 21.96 to 55U/mL across the experimental runs could be attributed to the differences in the combinations of levels at which each variable is present. ANOVA represented in Table 2 shows significant (probability 'p' < 0.05) positive effect of glucose (8.247), mustard oil cake (7.9), CASP (6.7) and casein (5.5) on subtilisin production. There is strong correlation observed for experimental and anticipated yields with coefficient of determination R² of 99.97% and 97.65% for experimental and predicted responses respectively that suggests good fit.

Equation 2 represents the regression analysis of first-order model.

Table 2
Examining Plackett-Burman Design for Subtilisin Production: Analysis of Variance.

Source	Coefficient	Effect	Degree of freedom	Sum of squares	Mean squares	F value	p value
Model			10	711.263	71.126	310.79	0.044*
Constant	34.902						0.003*
X ₁ -Casein	2.781	5.561	1	92.780	92.780	405.40	0.032*
X ₂ -NH ₄ Cl	0.708	1.416	1	6.014	6.014	26.28	0.123
X ₃ -NaCl	-0.293	-0.586	1	1.031	1.031	4.50	0.280
X ₄ -KH ₂ PO ₄	1.572	3.143	1	29.638	29.638	129.51	0.056
X ₅ -K ₂ HPO ₄	-0.248	-0.497	1	0.740	0.740	3.23	0.323
X ₆ -MgSO ₄	-1.245	-2.489	1	18.588	18.588	81.22	0.070
X ₇ -Yeast extract	-1.659	-3.318	1	33.037	33.037	144.35	0.053
X ₈ -Glucose	4.123	8.247	1	204.029	204.029	891.50	0.021*
X ₉ -Mustard oil cake	3.961	7.922	1	188.266	188.266	822.63	0.022*
X ₁₀ -CASP	3.381	6.761	1	137.140	137.140	599.23	0.026*
Residual error			1	0.229	0.229		
Total			11	711.492			

R² = 99.97%; Adjusted R² = 97.65%; F Fisher's function; Probability * (p < 0.05) corresponds to significance; CASP = Custard Apple Seed Powder.

$$Y = 34.902 + 2.781X_1 + 0.708X_2 - 0.293X_3 + 1.572X_4 - 0.248X_5 - 1.245X_6 - 1.659X_7 + 4.123X_8 + 3.961X_9 + 3.381X_{10} \quad (2)$$

Y is the predicted response and all the variables from X₁-X₁₀ are the coded forms of variables namely, casein, NH₄Cl, NaCl, KH₂PO₄, K₂HPO₄, MgSO₄, yeast extract, glucose, mustard oil cake and CASP.

The selection of variables for further optimization design by CCD-RSM was based on the assessment of PBD.

3.4. Optimization of subtilisin production by CCD-RSM

The designed matrix of CCD-RSM constituted of 31 experiments with four variables namely glucose (A), mustard oil cake (B), CASP (C) and casein (D) at five defined levels. Table 3 displays the levels of defined variables and experimental and predicted responses (subtilisin production U/mL). The responses were observed ranging from 28.2 to 70.5 U/mL and maximum production (70.5 U/mL) was seen with variables situated at central value '0'. Table 4 presents the ANOVA with 31.73 'F' value and significant model design. The linear variables namely, glucose, mustard oil cake and CASP, square terms and 2-way effects of glucose *CASP, glucose *casein, mustard oil cake*casein and CASP*casein were found to be significant for subtilisin production under the designed space. The coefficient of determination R² were 96.52% and 93.48% respectively for observed and predicted responses. There is a fair match between observed and expected responses in the present design and the model's adequacy for the current evaluation is depicted by a negligible lack of fit. Equation 3 for the second order polynomial model is demonstrated below.

$$Y = 69.82 + 11.79A + 3.7B + 2.86C - 5.49A^2 - 4.64B^2 - 5.76C^2 - 3.25D^2 + 3.12AC - 1.98AD + 3.07BD + 3.47CD \quad (3)$$

Where, Y indicates defined response (subtilisin production U/mL), A, B, C and are the coded values of glucose, mustard oil cake, CASP and casein respectively.

The significant interactions among the variables were evaluated by response surface plots demonstrated in Fig. 2D-G. The interaction among glucose and CASP was significant; Fig. 2D. Depicts elevation in subtilisin production with increased glucose concentration up to central value of 3% followed by decline at higher concentration and CASP of 3.5% was evidenced to produce maximum subtilisin. Fig. 2E. Reflects maximum production at 3% glucose and 3.5% casein above which decline was seen. Significant

Table 3
Central composite design of response surface approach design matrix of subtilisin producing factors.

Run No.	A Glucose (%)	B Mustard oil cake (%)	C CASP (%)	D Casein (%)	Subtilisin production yield (U/mL)	
					Experimental	Predicted
1	(-1)2.5	(-1)2	(-1)2.5	(-1)2.5	44.3 ± 0.8	39.6875
2	(1)3.5	(-1)2	(-1)2.5	(-1)2.5	60.4 ± 0.9	60.0958
3	(-1)2.5	(1)4	(-1)2.5	(-1)2.5	37.6 ± 1.1	43.1125
4	(1)3.5	(1)4	(-1)2.5	(-1)2.5	67.2 ± 0.2	65.3208
5	(-1)2.5	(-1)2	(1)3.5	(-1)2.5	32.5 ± 1.4	35.2958
6	(1)3.5	(-1)2	(1)3.5	(-1)2.5	69.2 ± 0.5	68.2042
7	(-1)2.5	(1)4	(1)3.5	(-1)2.5	31.6 ± 0.3	32.5708
8	(1)3.5	(1)4	(1)3.5	(-1)2.5	68.8 ± 1.6	67.2792
9	(-1)2.5	(-1)2	(-1)2.5	(1)3.5	28.2 ± 0.4	28.9958
10	(1)3.5	(-1)2	(-1)2.5	(1)3.5	41.2 ± 0.1	41.4542
11	(-1)2.5	(1)4	(-1)2.5	(1)3.5	42.5 ± 1.0	44.7208
12	(1)3.5	(1)4	(-1)2.5	(1)3.5	62.5 ± 1.3	58.9792
13	(-1)2.5	(-1)2	(1)3.5	(1)3.5	35.4 ± 0.4	38.5042
14	(1)3.5	(-1)2	(1)3.5	(1)3.5	69.7 ± 0.8	63.4625
15	(-1)2.5	(1)4	(1)3.5	(1)3.5	48.5 ± 0.7	48.0792
16	(1)3.5	(1)4	(1)3.5	(1)3.5	69.0 ± 0.9	74.8375
17	(-2)2	(0)3	(0)3	(0)3	29.2 ± 1.2	24.2667
18	(2)4	(0)3	(0)3	(0)3	67.0 ± 1.5	71.4333
19	(0)3	(-2)1	(0)3	(0)3	41.0 ± 0.9	43.8500
20	(0)3	(2)5	(0)3	(0)3	62.0 ± 0.6	58.6500
21	(0)3	(0)3	(-2)2	(0)3	40.0 ± 1.7	41.0167
22	(0)3	(0)3	(2)4	(0)3	54.0 ± 1.8	52.4833
23	(0)3	(0)3	(0)3	(-2)2	58.1 ± 0.9	58.3667
24	(0)3	(0)3	(0)3	(2)4	56.0 ± 0.3	55.2333
25	(0)3	(0)3	(0)3	(0)3	70.0 ± 0.5	69.8286
26	(0)3	(0)3	(0)3	(0)3	70.4 ± 0.2	69.8286
27	(0)3	(0)3	(0)3	(0)3	69.3 ± 1.0	69.8286
28	(0)3	(0)3	(0)3	(0)3	69.0 ± 1.1	69.8286
29	(0)3	(0)3	(0)3	(0)3	70.5 ± 0.4	69.8286
30	(0)3	(0)3	(0)3	(0)3	70.2 ± 0.3	69.8286
31	(0)3	(0)3	(0)3	(0)3	69.4 ± 0.7	69.8286

The mean ± standard deviation of triplicates is employed to represent each experimental value. CASP = Custard Apple Seed Powder.

Table 4
Analyzing Variance in subtilisin production using Central Composite Design of Response Surface Methodology.

Source	Coefficient	Degree of freedom	Sum of squares	Mean squares	F value	p value
Model		14	6595.77	471.13	31.73	0.000*
Constant	69.826					
Linear		4	3877.56	969.39	65.28	0.000*
A-Glucose	11.7917	1	3337.04	3337.04	224.72	0.000*
B-Mustard oil cake	3.7000	1	328.56	328.56	22.13	0.000*
C-CASP	2.8667	1	197.23	197.23	13.28	0.002*
D-Casein	-0.7833	1	14.73	14.73	0.99	0.334
Square		4	2113.20	258.30	35.28	0.000*
A ² -Glucose * glucose	-5.4946	1	542.80	863.34	58.14	0.000*
B ² - Mustard oil cake * mustard oil cake	-4.6446	1	416.39	616.89	41.54	0.000*
C ² -CASP * CASP	-5.7696	1	850.64	951.92	64.10	0.000*
D ² - Casein * casein	-3.2571	1	303.37	303.37	20.43	0.000*
2-way interaction		6	605.02	100.84	6.79	0.001*
AB- Glucose * Mustard oil cake	0.4500	1	3.24	3.24	0.22	0.647
AC- Glucose * CASP	3.1250	1	156.25	156.25	10.52	0.005*
AD- Glucose * Casein	-1.9875	1	63.20	63.20	4.26	0.056*
BC- Mustard oil cake * CASP	-1.5375	1	37.82	37.82	2.55	0.130
BD- Mustard oil cake * Casein	3.0750	1	151.29	151.29	10.19	0.006*
CD- CASP * Casein	3.4750	1	193.21	193.21	13.01	0.002*
Residual error		16	237.60	14.85		0.000 ^a
Lack of fit		10	235.50	23.55	67.47	
Pure error		6	2.09	0.35		
Total		30	6833.37			

R² = 96.52%; Adjusted R² = 93.48%; F Fisher's function; Probability * (p < 0.05) corresponds to significance; p^a corresponds to insignificance; CASP = Custard Apple Seed Powder.

interactions between 2%mustard oil cake and 3.5% casein revealed maximum production (Fig. 2F). 2.5% CASP and 3.5% casein was observed to induce maximum production and below and above a steep decline was observed (Fig. 2G). The curvature of the response plots aided to assess the most effective concentrations of the variables required for highest productivity. The optimized concentra-

tion obtained were 3% glucose, 2.5–3.5% CASP, 3.5% casein and 2% mustard oil cake. The experimental validations were conducted in triplicates under the optimized conditions and 72.9 U/mL of subtilisin production was obtained indicated a significant 7.67-fold enhancement in the production after optimization. The designed optimization process fitted the predicted response and authenti-

cated the designed variables. The design confirms the enhancement in subtilisin production significantly.

3.5. Subtilisin production kinetics

Subtilisin production (U/mL) kinetics from *B. subtilis* strain ZK3 was studied using the designed media obtained after optimization over a period of 4 days. The kinetics profile of subtilisin production, cell biomass, protein and reducing sugars are shown in Fig. 2H. Subtilisin production ranged from 25 to 77 U/mL with maximum production (77 U/mL) obtained on 3rd d. The residual substrate (glucose) reduced from 3% to 0.07% on 4th d and glucose consumption by the strain was substantially increased from 2nd d for cell growth. The cell biomass increased to 2.95 on 3rd d and almost remained static. Highest protein of 0.27 mg/mL was produced on 3rd d after which decline was evidenced. Kinetics revealed that the maximum subtilisin production occurred on 3rd and this was the optimum harvesting time.

3.6. Subtilisin-capped nanoparticle synthesis and characterization

The successful amalgamation of subtilisin from *B. subtilis* strain ZK3 with varied concentrations of 5 mM, 10 mM and 50 mM silver nitrate solution was proved by the alteration of the mixture's shade through light yellow to an intense brown. This was evidenced post-incubation and the mixed solution successfully facilitated the conversion of aqueous silver ions (Ag^+) into AgNP through reduction. The observed change in suspension color served as an initial indication of subtilisin-capped silver nanoparticle synthesis. The presence and quantification of AgNP were validated using a UV spectrophotometer. Upon exposure to UV radiation, the recorded peak at 425 nm for 5 mM and 10 mM and 450 nm for 50 mM confirmed the presence of AgNP, as their characteristic range typically falls between 400 and 470 nm. The absorption spectra are plot and displayed in the Fig S2 in SI. The existence of unbound electrons within nanoparticles plays a role in generating a surface plasmon resonance (SPR) band. The coordinated vibrations of the independent electrons found in the AgNP are accountable for this band, which resonate with the incident light's fluctuating electric field.

ZnONP synthesis was initiated by introducing a 10 mM zinc acetate solution to subtilisin. The reaction mixture underwent a color change from the initial state to a yellowish color, eventually resulting in the formation of a cream-colored precipitate. This change in color was attributed to the occurrence of SPR in the ZnONP, indicating the successful formation of ZnONP. Both the formation of subtilisin-capped ZnONP and the reduction of Zn^{2+} ions to ZnONP were monitored using UV-Visible spectroscopy. Mei's hypothesis suggests that if a synthesized nanoparticle has merely one absorption peak in the UV-Vis spectra, it is likely to have a spherical shape. The emergence of a large peak in the ultraviolet-visible spectrum extending from 300 to 400 nm, indicates the existence of zinc oxide nanoparticles. A substantial peak at 380 nm was identified in this investigation, demonstrating the generation of zinc oxide nanoparticles in the combination (Fig S2 in SI). The presence of a narrow peak suggests a high degree of homogeneity and uniformity in the synthesized zinc oxide nanoparticles, indicating a well-controlled biosynthesis process.

3.7. Functional characterization of subtilisin capped silver and zinc oxide nanoparticles

3.7.1. Evaluation of antibacterial activity and MIC

Antibiotic-resistant microorganisms are becoming increasingly common, posing a severe danger to public health, as it limits the effectiveness of existing treatment options. To combat this chal-

lenge, the development of alternative antimicrobial agents is essential. Naturally derived products, plant-based extracts, nanoparticles, and peptides that inhibit microbes are used as active components in the manufacture of affordable antimicrobial agents. The antimicrobial activity of nanoparticles is attributed to multiple mechanisms, including physical disruption of microbial membranes, oxidative stress caused by the formation of reactive oxygen species (ROS), interference with cellular signalling pathways and disruption of essential metabolic processes. In the current study, antibacterial efficiency and MIC of subtilisin and subtilisin-capped AgNP and ZnONP were investigated against three Gram-positive and Gram-negative pathogens respectively. The antibacterial property of nanoparticles generated by biosynthesis was demonstrated to be effective against all pathogens examined in this study. Table 5 explains that subtilisin displayed maximum clearance zone (mm) against *B. licheniformis* (17 ± 0.3 mm) and *E. coli* (18 ± 0.9 mm) compared to *B. cereus* (13 ± 0.2 mm) and *S. aureus* (15 ± 0.5 mm) for Gram-positive bacteria and *P. aeruginosa* (16 ± 0.1 mm) and *S. typhimurium* (15 ± 0.4 mm) for Gram-negative bacteria. Pronounced activity was evidenced for subtilisin-capped AgNP 50 mM and ZnONP 50 mM with the latter being highly inhibited for *B. licheniformis* (23 ± 0.1 mm) and *E. coli* (25 ± 0.6 mm) respectively. *B. cereus* showed slight lower inhibition for the capped nanoparticles. The impact of the capped nanoparticles on the growth of each tested pathogen was unique and differs from one organism to another. The observed suppression of pathogen development implies that silver ions were released from the metallic nanoparticles (AgNP). Subtilisin acts as a bio-control agent, facilitating the diffusion of silver ions through the solidified agar layer, thereby impeding the proliferation of pathogenic populations in the agar medium. The positive control, cefixime, exhibited zones of inhibition ranging from 15.2 ± 0.4 to 27.6 ± 0.7 mm, as shown in Table 5.

Table 6 shows the summary of MIC of subtilisin and subtilisin-capped AgNP and ZnONP against Gram-positive and Gram-negative pathogens. It was performed using the standard microbroth dilution method by following CLSI guidelines. Among all the pathogens, capped ZnONP depicted lowest MIC of 3.125 mM against two pathogens namely *B. cereus* and *B. licheniformis* proving it to be excellent antibacterial agent. AgNP has also shown similar MIC against *B. licheniformis*. This reveals that the subtilisin-capped nanoparticles have enhanced the antibacterial effect when compared to the effect of the protein alone.

3.7.2. Assessment of antioxidant activity

The presence of antioxidants in nanoparticles provides notable advantages by shielding against oxidative stress, amplifying therapeutic effectiveness, conserving bioactive substances, fostering skin well-being, safeguarding the ecosystem, lessening cellular toxicity, and facilitating applications in biomedicine. Integrating antioxidants into nanoparticles enhances their capacity across various sectors and fields in biomedicine, contributing to overall health improvement and wellness. In the present research, the antioxidant activity of subtilisin and subtilisin-capped AgNP and ZnONP were studied using DPPH and ABTS radical scavenging assays. Both methods used in this study were characterized by their ease of use, rapidity, sensitivity and ability to produce excellent results in assessing the radical scavenging activity of biosynthesized nanoparticles. DPPH, an organic radical commercially available, typically possesses a purple color. However, upon reduction, the purple color of DPPH fades, indicating the antioxidant capacity of the substance being tested. The radical scavenging activity of subtilisin and nanoparticles was dependent upon dose, i.e., their % effectiveness increased as the drug concentration rose. The scavenging activity ranged from 18 to 65% for subtilisin with 25–150 $\mu\text{g/mL}$ concentration range showing highest at 150 $\mu\text{g/}$

Table 5
Antibacterial activities of subtilisin and subtilisin capped AgNP and ZnONP against Gram-positive and Gram-negative pathogens.

AMA		Gram positive bacterial strains			Gram negative bacterial strains		
		<i>Bacillus cereus</i>	<i>Staphylococcus aureus</i>	<i>Bacillus licheniformis</i>	<i>Pseudomonas aeruginosa</i>	<i>Escherichia coli</i>	<i>Salmonella typhimurium</i>
Inhibition zone diameter (mm ± SD)	Subtilisin	13 ± 0.2	15 ± 0.5	17 ± 0.3	16 ± 0.1	18 ± 0.9	15 ± 0.4
	AgNP	11 ± 0.5	12 ± 0.2	15 ± 0.8	15 ± 0.2	13 ± 0.8	14 ± 0.6
	10 mM						
	AgNP	18 ± 0.7	22 ± 0.6	20 ± 0.4	17 ± 0.5	19 ± 0.5	18 ± 0.8
	50 mM						
	ZnONP	12 ± 0.9	9 ± 0.2	13 ± 0.6	14 ± 0.9	17 ± 0.7	16 ± 1.1
	10 mM						
ZnONP	21 ± 0.1	20 ± 0.3	23 ± 0.1	22 ± 1.0	25 ± 0.6	21 ± 0.3	
50 mM							
Cefixime		20.3 ± 0.6	15.2 ± 0.4	27.6 ± 0.7	15.6 ± 0.9	18.9 ± 0.7	15.2 ± 0.5

Table 6
Minimum inhibitory concentration (MIC) of subtilisin and subtilisin capped AgNP and ZnONP.

MIC		Gram positive bacterial strains			Gram negative bacterial strains		
		<i>Bacillus cereus</i>	<i>Staphylococcus aureus</i>	<i>Bacillus licheniformis</i>	<i>Pseudomonas aeruginosa</i>	<i>Escherichia coli</i>	<i>Salmonella typhimurium</i>
MIC (µg/mL)	Subtilisin	37.5	37.5	9.375	18.75	9.375	37.5
MIC (mM)	AgNP	6.25	12.5	3.125	12.5	6.5	12.5
	ZnONP	3.125	12.5	3.125	6.5	12.5	6.5

mL. Maximum inhibition was observed at 89% for ascorbic acid as the reference standard as displayed in Table 7. The outcomes of AgNP and ZnONP have been compiled in Table 7 and depict that subtilisin-capped ZnONP have exhibited the highest scavenging activity when compared to subtilisin-capped AgNP and subtilisin alone. It displayed significant inhibition of 80% even after 30 min. incubation while AgNP showed 60% at 50 mM concentration.

Another radical activity named ABTS was also studied for subtilisin and its capped nanoparticles. During the 12 to 60 h period, an inhibition percentage ranging from 18% to 90% was observed. The maximum inhibition percentage of 90% was recorded at the 60 h time point for ZnONP (Fig. 3A). The same concentration of AgNP showed 45% scavenging activity at 60 h and subtilisin at 40%. Butylated hydroxytoluene was used as standard, showing inhibition of 46%. According to the study, all sample dosages demonstrated excellent scavenging of free radicals' capabilities. However, it was observed that ZnONP have given outstanding results in the case of both assays revealing it to be a potential antioxidant. All of the experiments reported in the study were performed in triplicates, and the mean value of the three separate batches was used to determine the final results, ensuring statistical reliability and reducing the impact of any potential variability or outliers in the data.

3.7.3. Evaluation of anticancer activity

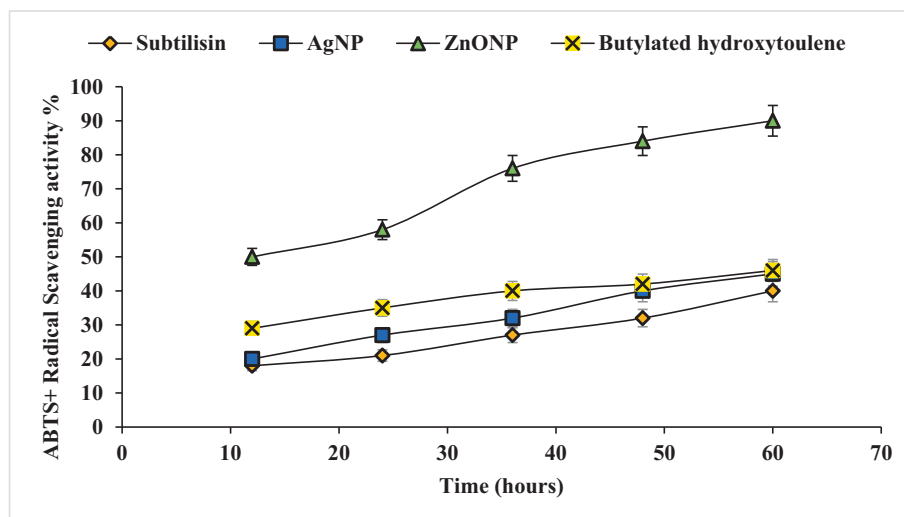
The MTT assay holds great significance and is extensively employed in anticancer research. Its capacity to evaluate cell via-

bility and cytotoxicity of compounds makes it indispensable for screening potential anticancer agents and gaining a valuable understanding of their anticancer activity. Cancer cells with reduced viability due to the cytotoxic effects of anticancer agents will display lower MTT assay results, indicating potential anticancer activity. The cytotoxic activity of subtilisin and subtilisin-capped nanoparticles were examined against MCF-7 cancerous cell lines *in-vitro*. The concentration of the samples ranged between 6.25 and 200 µg/mL and the cell viability percentage was determined. Fig. 3B shows the dose-dependent significant decrease in the viability of the treated samples. Cell viability decreased as the concentration of both subtilisin and its capped nanoparticles increased and ZnONP exhibited higher activity than AgNP. The MCF-7 cell lines' IC₅₀ value, which represents the true dose of subtilisin, was established. The concentrations of AgNP and ZnONP required to limit cell growth by 50% have been estimated (Sarkar and Kotteeswaran, 2018) to be 83.48 µg/mL, 3.62 µg/mL and 7.57 µg/mL respectively. The rate of viable cells was drastically decreased at concentrations exceeding 40 µg/mL. Doxorubicin served as the control drug having IC₅₀ value of 3.62 µg/mL which aligned with the trend of AgNP. Subtilisin drastically exhibited a decrease in viability (67.22%) after 50 µg/mL concentration. Our research findings confirmed the anti-cancer potential of nanoparticles particularly AgNP and concluded that AgNP were more effective than others in inhibiting cancer cell growth.

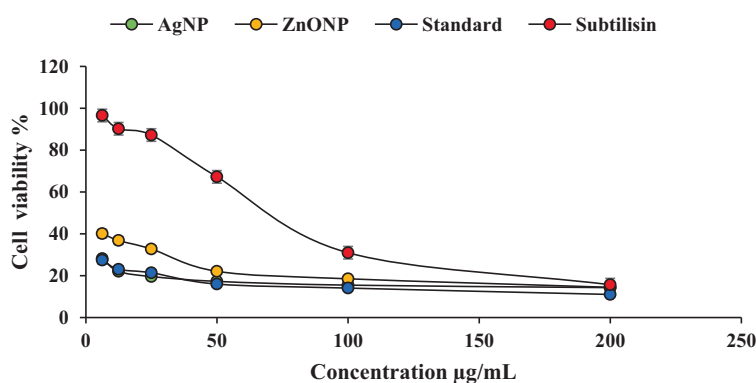
Table 7
DPPH radical scavenging assay of subtilisin and subtilisin-capped AgNP and ZnONP.

Subtilisin		AgNP		ZnONP		Ascorbic acid	
Concentration (µg/mL)	Scavenging activity (%)	Concentration (mM)	Scavenging activity (%)	Concentration (µg/mL)	Scavenging activity (%)	Concentration (µg/mL)	Scavenging activity (%)
25	18 ± 0.09	5	14 ± 0.07	10	36 ± 1.0	10	68 ± 0.03
50	21 ± 0.10	10	24 ± 0.03	20	40 ± 0.5	20	71 ± 0.09
75	35 ± 0.03	20	33 ± 0.08	30	53 ± 1.2	30	77 ± 0.5
100	46 ± 0.5	30	44 ± 1.0	40	64 ± 0.08	40	82 ± 1.1
125	57 ± 1.0	40	53 ± 1.1	50	72 ± 0.03	50	86 ± 0.1
150	65 ± 0.7	50	60 ± 0.05	60	80 ± 0.04	60	89 ± 0.06

Each data value represents mean ± standard deviation value of triplicates and significant at $p < 0.05$.



(A)



(B)

Fig. 3. Biological activities of subtilisin and subtilisin-capped AgNP and ZnONP. Antioxidant activity of subtilisin and subtilisin-capped AgNP and ZnONP by ABTS assay (A), Cytotoxicity activity of subtilisin and subtilisin-capped AgNP and ZnONP against breast cancer cell lines (B).

3.8. Analytical characterization

3.8.1. FTIR analysis of subtilisin-capped nanoparticles

The significant functional groups of the bio-synthesized subtilisin-capped Ag and ZnO nanoparticles have been studied using FTIR approach. The FTIR spectrum of nanomaterials revealed a number of major bands, each suggesting an existence of unique functional groups of subtilisin and nanoparticles as shown in Fig. S3 (A) and (B) in SI. The existence of a carboxylic acid counterpart with an amine group amidst amino-acid residues in proteinous molecules indicates the presence of the infrared portion of the electromagnetic radiation spectrum. In Fig. S3A in SI, the confirmation of the N–H stretching mode is evident from the presence of amide bands at a broad absorption peak of 3394 cm^{-1} . At approximately 2924 cm^{-1} , aliphatic C–H vibrations are evidenced. The alkyne symmetric stretch of $\text{–C}\equiv\text{C}$ bonds typically occurred nearly at 1577 cm^{-1} in the infrared spectrum. The Amide II band is centred at 1577 cm^{-1} , while the Amide III band is centred at 1384 cm^{-1} . The major signal used for recognizing protein secondary structures is typically found in the amide I region of the infrared spectrum, which is around $1350\text{–}1750\text{ cm}^{-1}$. The amide I band provides important information about the protein's alpha-helical, beta-sheet and random coil secondary structures, making

it a key region for structural analysis using FTIR spectroscopy. The $\text{–C}\equiv\text{N}$ extension of amines with an aliphatic structure or phenolic/alcoholic compounds correlates to the peak at 1077 cm^{-1} in the silver nanoparticle FTIR spectra as shown in Fig. S3A in SI. This absorption band suggests the existence of these particular functional groups, which might be ascribed to the capping agents or stabilizers utilized during the silver nanoparticles synthesis. The striking peak at 536 cm^{-1} was attributed to Ag–O vibrations (Fouad et al., 2017). The presence of silver ions and oxygen-containing functional groups, typically associated with silver nanoparticles, is indicated by the peak. This peak provides valuable information about the formation of Ag nanoparticles and the specific chemical bonds present in the material.

The FTIR spectrum displayed multiple absorption peaks, as displayed in Fig. S3B in SI, indicating the presence of a specific biological substance that played a role in the biosynthesis of zinc oxide nanoparticles. These absorption peaks offer insight on the structure and composition of the biomolecules participating in the procedure of synthesis and help to characterize ZnONP formation. The –OH extension comprising phenolic or alcoholic compounds is allocated to the typical peaks at 3344 cm^{-1} whereas the peak at 1654 cm^{-1} corresponds to the C–O stretch. The long peak at 1048 cm^{-1} corresponds to vibrations of C–C, C–OH and C–H

functional groups. Additionally, the FTIR spectrum of the biosynthesized ZnONP revealed a distinct band at 597 cm^{-1} , which signifies the existence of ZnO vibrations. This absorption peak provides strong evidence for the formation of zinc-oxygen bonds in the ZnO nanoparticles and supports the successful biosynthesis of ZnONP as a result of which metallic ions are reduced to metallic nanoparticles (Alahdal et al., 2022).

3.8.2. SEM-EDS analysis of subtilisin capped nanoparticles

It is a technique for analysis that makes use of a scanning electron microscope, also called as SEM, to acquire high-resolution photographs of a sample's surface morphology. EDS analyses the composition of elements by detecting X-rays generated by the specimen when it gets struck with an electron beam. SEM-EDS is extensively utilized to explore the topological morphology and chemical composition of an array of samples in the fields of materials science, nanotechnology and other scientific domains. The dried nanoparticles were observed under SEM. Fig. 4 depicts the nano-composite agglomerates of ultra-small-sized silver nanoparticles co-embedded with subtilisin. They were bacilli like structure and curved shaped. The formation of agglomerates could have occurred during the drying process. This was validated further by the EDS study shown in Fig. 4B as there was presence of silver component in the spectra of AgNP. The diminishment of silver ions Ag^+ to Ag^0 was confirmed by an elevated peak observed at 3 keV (binding energies), corresponding to the existence of silver ions in the reduced state. The spectra revealed that silver was the most predominant element, accounting for 37.60% of the total, followed by carbon (32.13%) and oxygen (24.68%) and impurities (5.59%), indicating the creation of silver nanoparticle capped subtilisin (data not shown) (Fouad et al., 2017).

Similarly, surface morphology of subtilisin-capped ZnONP exhibited a spherical morphology with elongated rods, but having an uneven texture with a slightly even and regular dispersion to understand their structure and potential applications (Fig. 4C).

EDS data may be used to confirm ZnONP purity and composition. It typically showed a strong signal for zinc (Zn) and oxygen (O) elements, confirming the presence of ZnO in the sample between 8.6 keV and at 0-1 keV, respectively as shown in Fig. 4D. Furthermore, EDS may also identify additional elements present as impurities or as components of the stabilizing or capping agents utilized during nanoparticle development. The EDS spectra revealed the highest component to be Zn with 91.01% followed by oxygen to be 1.18% and other substances. (data not shown) (Alahdal et al., 2022).

3.8.3. TGA analysis of subtilisin-capped nanoparticles

TGA can offer valuable data with regard to their thermal resistance as well as the existence of residual impurities or organic molecules on their surfaces. Through monitoring the sample's weight changes during heating, TGA aids researchers in comprehending the thermal characteristics and composition of nanoparticles. This information holds great significance for diverse applications in nanotechnology, nanomedicine and materials science. Specific stages of weight loss were observed during the TGA analysis. In Fig. 4E, at the initial stage of weight loss (<200 °C), a relatively small decrease of 0.99% was observed, which is linked to the evaporation of physisorbed water or surface moisture content on the AgNP. The second phase of reducing weight at 12.77% occurs between 200 and 570 °C, and involves the decomposition and volatilization of organic and bioactive compounds that might be present on the sample, such as surfactants, stabilizers, or capping agents. Additional weight loss can be observed when inorganic components undergo decomposition, leading to the release of gases and volatile byproducts (Alam, 2022). Post 600 °C at elevated temperatures, the silver nanoparticles at this stage represent capped silver nanoparticle core material decomposition. It stabilizes after a minimal loss. The biosynthesized AgNP are estimated to have a purity of approximately 73.47% pure silver.

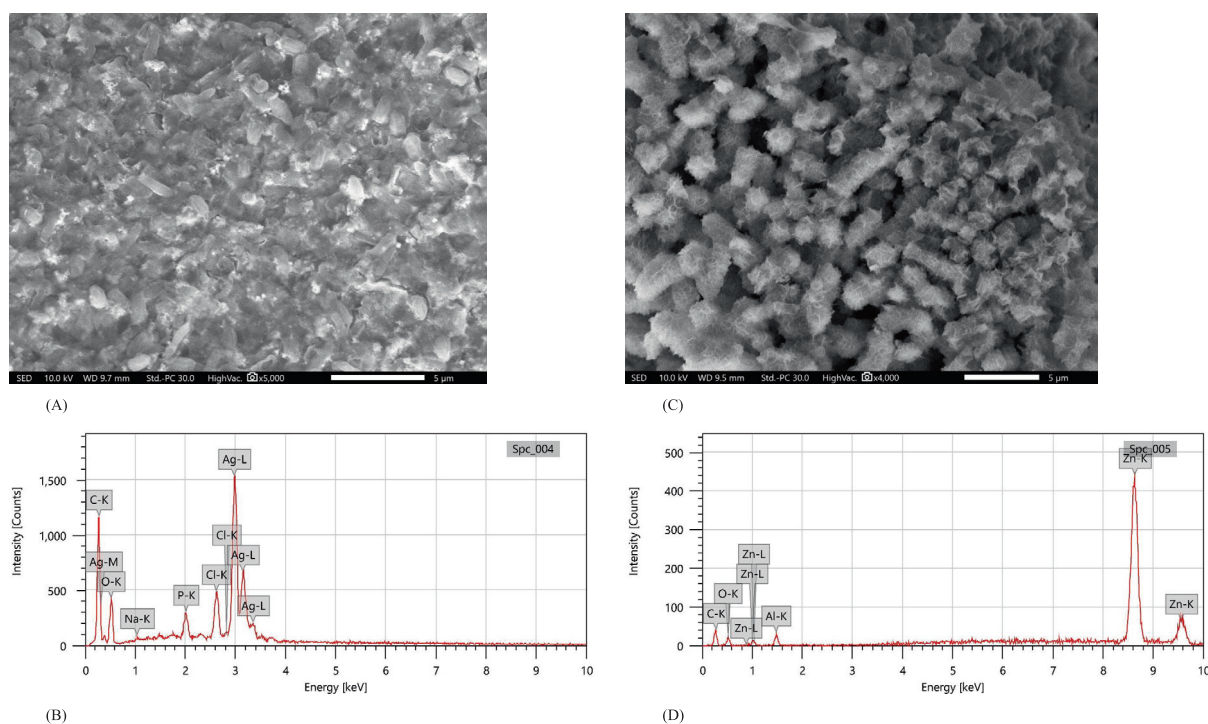
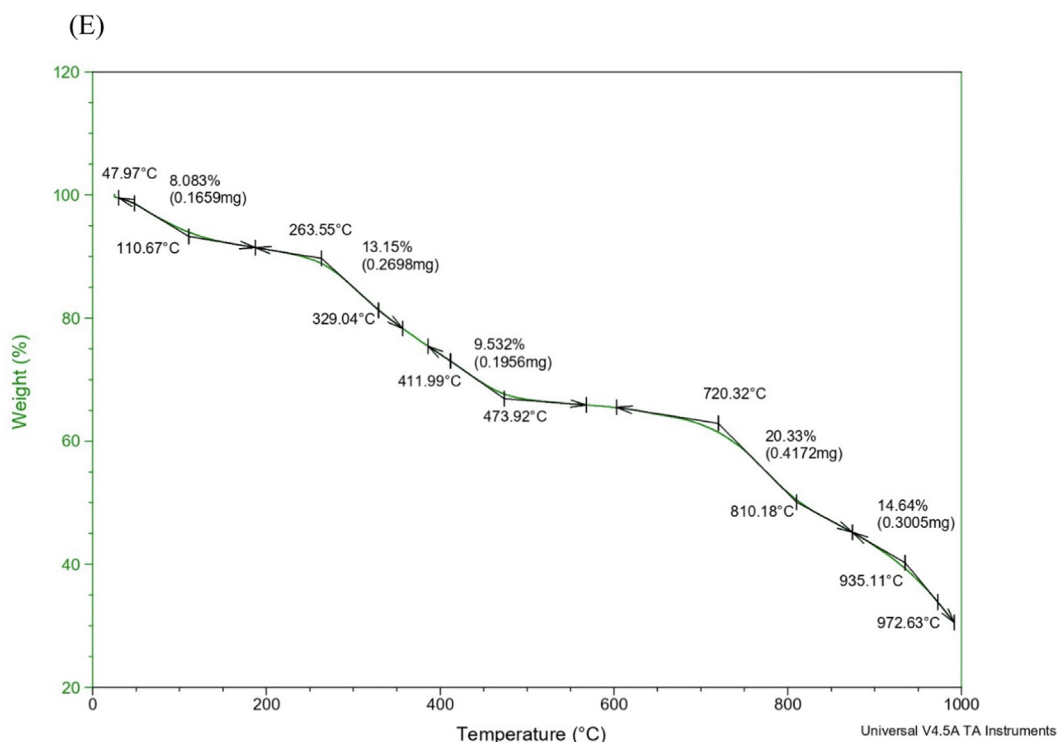
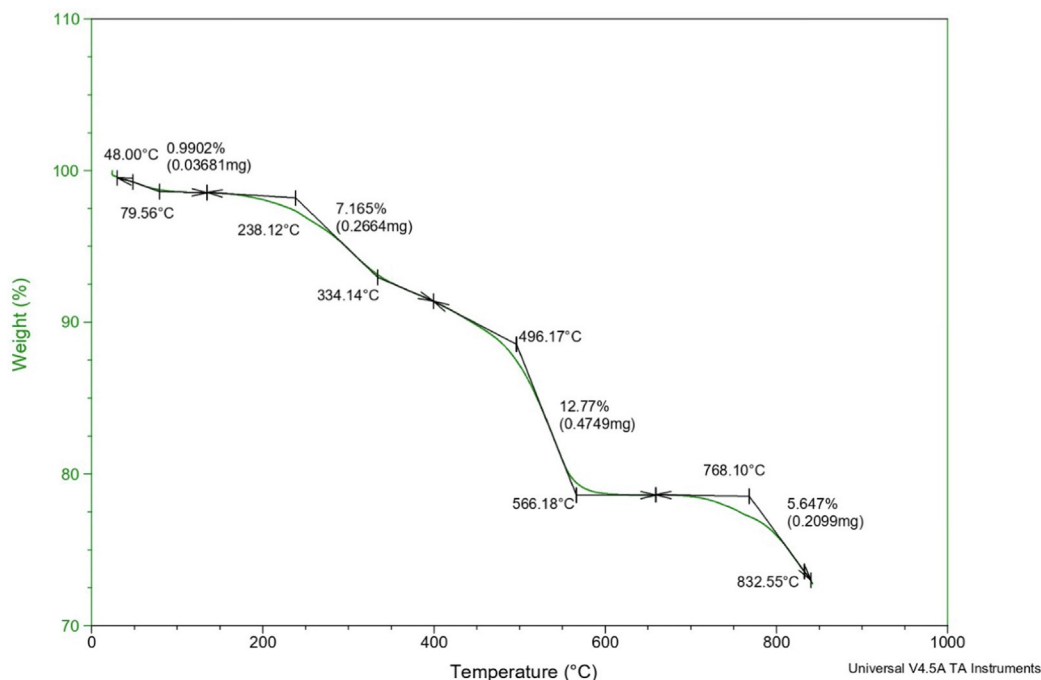


Fig. 4. Analytical characterization of subtilisin-capped AgNP and ZnONP. SEM analysis of AgNP-subtilisin (A), EDS of AgNP-subtilisin (B), SEM analysis of ZnONP-subtilisin (C), EDS of ZnONP-subtilisin (D), TGA analysis of AgNP-subtilisin (E), TGA analysis of ZnONP-subtilisin (F), AFM micrographs of subtilisin-capped AgNP (G), AFM micrographs of subtilisin-capped ZnONP (H), XRD diffractogram of subtilisin-capped AgNP (I) and XRD diffractogram of subtilisin-capped ZnONP (J).

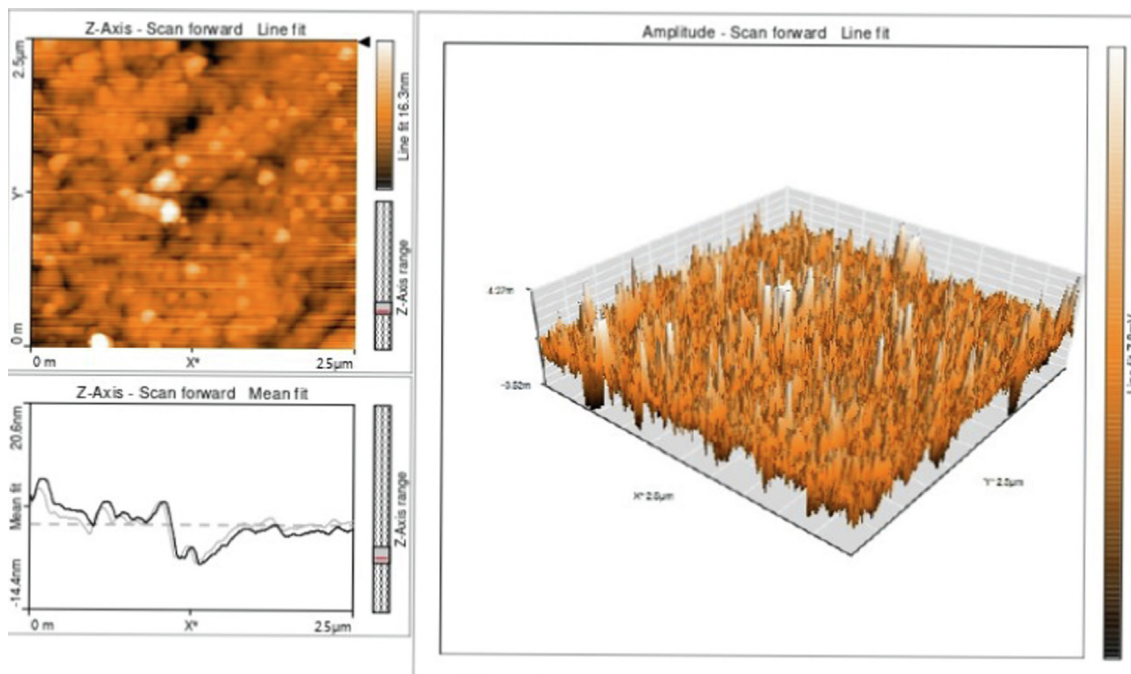


(F)

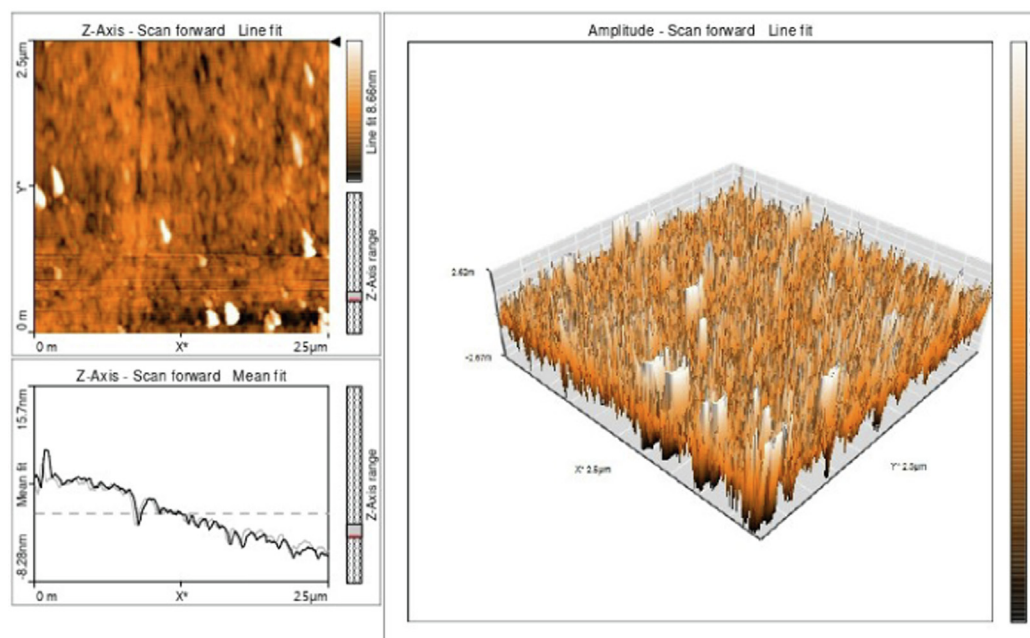
Fig. 4 (continued)

Similar weight loss stages were also seen in subtilisin-capped zinc oxide nanoparticles as shown in Fig. 4F. The first stage of weight loss between room temperature to 263 °C depicted a minor loss of 8.083% which could suggest the reason for water molecules loss present on the surface of nanoparticles. There is a significant decline in weight by 9.53% at 473 °C, ascribed to the molecule's degradation and evaporation. The absence of residues at approxi-

mately 600 °C suggested that the subtilisin-capped ZnONP structure had decomposed into gases and also results in the development of carbonaceous char. At 953 °C, 14.64% weight loss was observed indicating the additional decomposition and evaporation of the remaining bioactive molecule. At this temperature, the majority of organic compounds and impurities are expected to have been eliminated, resulting in the production of highly puri-



(G)



(H)

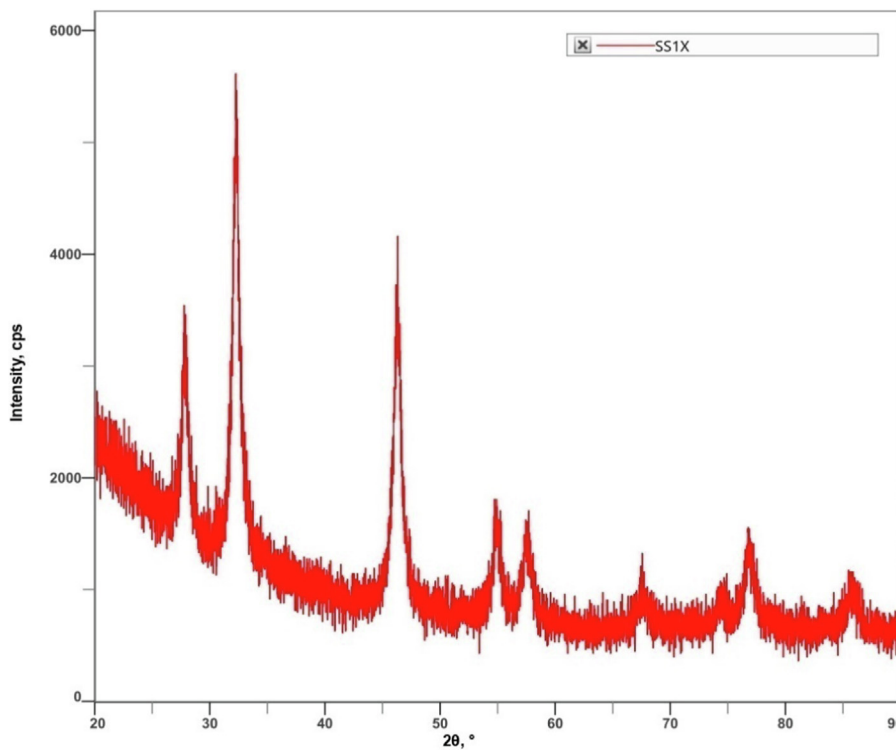
Fig. 4 (continued)

fied zinc nanoparticles (Özbek and Ünal, 2017). The TGA curve displays a substantial reduction in weight as any remaining materials are expelled, and the sample approaches its utmost thermal stability. The final weight of the sample at around 900 °C will indicate the pure zinc oxide content of the nanoparticles.

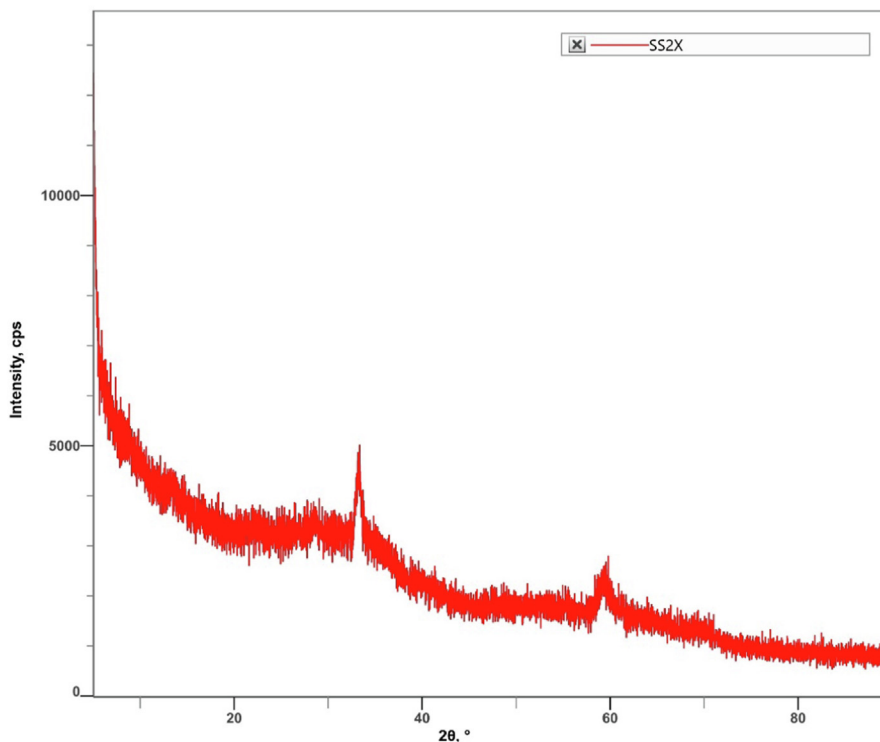
3.8.4. AFM analysis of nanoparticles

AFM allows researchers to produce high-resolution images and height profiles by scanning a sharp tip across the surface of

nanoparticles. This enables the visualization of individual nanoparticles and the way they cluster together, aiding in the characterization of their physical properties. As the AFM tip is coupled to a bendable cantilever, the cantilever bends owing to attraction and repulsive interactions between the molecules and atoms on the tip and its exterior surface, when the tip hits the sample ground. The deflection of the cantilever is then measured, and a feedback mechanism is used to maintain a constant force between the tip and the sample. The silver and zinc nanoparticles of capped sub-



(I)



(J)

Fig. 4 (continued)

isin were analyzed by AFM to study its detailed morphology and agglomeration. The AFM micrograph of AgNP depicted formation of agglomerates with spherical morphology and uniform distribution in Fig. 4G. The actual appearance of the AgNP is based on the

experimental setup, sample preparation and imaging parameters (Thiruchelvi et al., 2021).

AFM was employed to characterize the 2D and 3D topography of the biosynthesized ZnONP. This allowed for detailed visualiza-

tion and analysis of the surface features of the nanoparticles at the nanoscale. AFM images provided visual insights into the roughness and morphology of the surface for the zinc oxide nanoparticles biosynthesized using subtilisin from *B. subtilis* strain (Fig. 4H). The 3D image of the film reveals a consistent and ordered composition, with the grains exhibiting a vertical structure along the crystal axis. The grains appear to be relatively uniform in size and shape, indicating a regularity in the bioactive capped nanoparticle composition (Rajeswaran et al., 2019). This suggests that the distribution of nanoparticles was even, and the homogeneity within the scanned region was adequate.

3.8.5. X-ray diffraction analysis of nanoparticles

XRD of subtilisin-capped nanoparticles is a powerful analytical technique used to figure out their crystal structure and identify the crystalline phases that existing in the sample. By subjecting the nanoparticles to X-ray radiation, the XRD pattern produced provides valuable information about the arrangement of atoms in the nanoparticles, their lattice spacing, and their crystallographic orientations. The diffractogram exhibited several Bragg reflections, which have been indexed according to the face-centered cubic grain structure of silver. These reflections correspond to the specific crystallographic planes and orientations present in the silver nanoparticles, providing valuable information about their crystalline structure. The XRD diffractogram revealed 4 prominent peaks at 2θ values ranging between 20 and 90° at 32.28 , 46.27 , 67.37 , and 76.74 , which have been attributed to the existence of silver metal (Fig. 4I). These peaks could be associated with the crystallographic planes of (1 1 1), (2 0 0), (2 2 0), and (3 1 1) of the silver nanoparticles. The appearance of these specific peaks confirms the face-centered cubic crystal structure of silver in the synthesized nanoparticles. By comparing the XRD spectrum with the standard JCPDS (Joint Committee on Powder Diffraction Standards) file number 89–3722, it was verified that the silver biosynthesized in our experiments exists in the nanocrystal form. This comparison confirms the crystalline nature and nanoscale structure of the synthesized silver nanoparticles, aligning with the reference pattern provided by the JCPDS database (Jan et al., 2021). Many resilient extra Bragg peaks were found in the XRD spectrum near the typical peaks. These peaks were not specifically assigned and could be attributed to the presence of some bioorganic compound (s) or protein (s) found in the mixture. The appearance of these unassigned peaks indicates the possibility of some additional molecular interactions or phases within the biosynthesized nanoparticles, possibly due to the bioorganic compounds or proteins that may have been involved in the nanoparticle synthesis process. Further analysis and investigation are required to determine the exact nature and contribution of these additional peaks (Omole et al., 2018). The average subtilisin-capped AgNP size was identified by the Debye-Scherrer formula and found to be approximately 10.16 nm. The formula is as follows:

$$D = k\lambda/\beta\cos\theta \quad (4)$$

where D is the mean crystallite size (nm), k is the Scherrer constant (here $k = 0.9$), λ is the X-ray wavelength (wavelength is 1.54 \AA), θ is the Bragg angle (2θ), and β is the full width at the half maxima (radian) (Alam, 2022; Shankar et al., 2020).

The XRD pattern of subtilisin-capped ZnONP showed crystalline structure with average particle size computed from equation 4 to be 3 nm. The analysis of the characteristic peaks in the XRD pattern at 33.19 , 54.33 , 59.19 and 69.15 confirmed that all the observed peaks corresponded to ZnONP as shown in Fig. 4J. The existence of more powerful peaks associated with the 101 planes, which are positioned at roughly 33.19° , suggests a high degree of crystallinity in the ZnONP. No indications of impurities were found in the synthesized ZnONP, suggesting a high level of purity in the

nanoparticles. The absence of additional peaks or impurity signals reinforces the notion that the synthesized ZnONP are of high quality and possess a well-defined crystal structure, enhancing their potential for various applications in nanotechnology and materials science (Faisal et al., 2021).

4. Discussion

The successful isolation of *B. subtilis* strain ZK3 has been explained in this work, from a novel source of marine soil which showed a high resemblance to *B. subtilis* based on the phylogenetic analysis. Multiple researchers have documented the isolation of different strains from diverse sources. Alkaline proteases are produced by a diverse range of organisms. *Bacillus* species, in particular, are commonly associated with production of proteases available commercially (Mahmoud et al., 2021). Major *Bacillus* species have been found in the soils which are capable of producing alkaline and serine proteases (El-Bendary et al., 2021) isolated *B. subtilis* strain NRC1 from an old golden earring that showed positive for casein assay. *B. aryabhatai* Ab15-ES was discovered from effluent of poultry processing revealing a clear zone of caseinolytic activity on skim milk agar plate (Adetunji and Olaniran, 2020). *B. cereus* was identified from soil that was organic at Karicode, Kollam (Kerala) and found to possess the capability of producing alkaline protease (Thomas et al., 2021). A psychrotrophic *B. pumilus* BO1 from Tajwas Glacier of Kashmir, India showed hydrolysis zone on the casein plate (Farooq et al., 2021). Alkaline protease producer *B. subtilis* D9 from Saudi Arabia is reported (Mahmoud et al., 2021). *Bacillus* sp. BT MASC 3 strain was isolated from waste dumping site soil and subtilisin, a kind of serine protease was studied (Kandasamy et al., 2016). However, strains reported specifically for subtilisins are few.

Subtilisin-like serine protease and alkaline protease production have been reported by several workers. In the present research work, CASP was discovered to be an intriguing carbon source and mustard oil cake was nitrogen rich source to induce high subtilisin production in *B. subtilis* strain ZK3. In an interesting study by Elumalai et al. (2020), *B. subtilis* B22 produced protease during submerged fermentation under different lights and found light-emitting diodes to maximize the production using casein as substrate. Maltose and yeast extract were discovered to be better carbon and nitrogen sources respectively for protease production by *Streptomyces* sp. Al-Dhabi-82 (Abdullah Al-Dhabi et al., 2020). The big confront in the fermentation process is the cost involved in the usage of commercial media ingredients employed for the production of high value products like enzymes. Hence, the objective is to lower the production cost by using low-cost wastes and byproducts that can enhance the yields. The substrate that supports the microbial growth owing to the rich nutritional composition of minerals and cofactors are preferred as they support in the biosynthesis of microbial metabolites. The nature and composition of substrate constituting the carbon and nitrogen part can greatly influence the expression of hydrolytic enzymes during fermentation processes. It is reported that agricultural waste residues like groundnut oil cake, soybean meal, coconut oil cake and linseed oil cake have high content of carbohydrates and proteins that can serve as better fermentation substrates for protease production (Elumalai et al., 2020) and are natural sources. Elevated protease production was observed on 3rd day using feather meal substrate by *Bacillus* sp. CL33A (Clerici et al., 2021). *Gliricidia sepium* seed flour as nitrogen rich substrate was used to produce serine protease from *Paenibacillus graminis* MC 2213 with 15.9 U/mL during 96 h of submerged fermentation (Couto et al., 2022). Groundnut oil cake as agricultural waste product showed improved protease production by *B. subtilis* B22 (Elumalai et al., 2020). In a study,

organic municipal solid wastes rich in cellulose and protein wastes were replaced for commercial carbon (glucose) and nitrogen (peptone and yeast extract) sources and found comparable protease production indicating adequate replacement to commercial sources from *B. subtilis* AKAL7 and *Exiguobacterium indicum* AKAL11 (Hakim et al., 2018). The suitable carbon and nitrogen sources were fructose and glucose and shrimp shell powder respectively for protease from *B. luteus* H11 (Kalwasińska et al., 2018). Substrates like de-oiled neem seed cake was employed to produce protease (11–12 U/mL) and addition of other carbon (sucrose and fructose) and nitrogen (yeast and urea) sources favored a substantial increase in the production by *B. licheniformis* and *Acinetobacter pittii* (Reddy et al., 2022). Wheat bran, as an agro-waste, was uncovered to serve as a superior substrate for manufacturing via solid-state fermentation by *Mycothermus thermophilus* MK770356 fungi possibly due to the rich content of nutrients and cofactors (Talhi et al., 2022). The utilization of an alternative agricultural waste as a new inducer in the media, Custard Apple Seed Powder (CASP) demonstrated a substantial 1.88-fold increase in alkaline protease synthesis by *Neocosmospora* sp. N1. (Matkawala et al., 2019).

The feasibility of multiple agricultural byproducts as substrates for protease synthesis from *Bacillus halodurans* included, paddy husk, rice meal, straw from paddy fields, fruit and vegetables waste, the bran of wheat, and sawdust (1% each), was investigated. The study states that in the experiment, among the tested substrates, medium enriched with wheat bran supplementation resulted in the highest enzyme yield. On the other hand, sawdust supplementation resulted in the lowest enzyme yield. This indicates that wheat bran was the most effective substrate for promoting the production of the enzyme, while sawdust was less effective in comparison (Balachandran et al., 2021). Another research delved into the utilization of cow dung as an interesting and budget-friendly alternative for the concurrent creation of carboxy methyl cellulase (CMCase) and protease from a novel *B. subtilis* IND19. This economical substrate holds the promise of diminishing the expenses linked to enzyme generation. This was the first study to investigate the simultaneous production of two enzymes in solid state fermentation (Vijayaraghavan et al., 2016).

PBD proposes quick mathematical computing that aids in filtering of important and crucial factors from an array of factors necessary for optimization. PBD recommended the following major parameters in the current study: glucose, mustard oil cake, CASP and casein for further optimization. In consent with our results, glucose along with soybean protein and temperature were found to be effective for production of alkaline serine protease by *B. safensis* (Elyasi Far et al., 2020). Previous reports suggest a 1.15-fold improvement in the enzyme activity with 25.3 U/mL based on PBD by *B. cereus* KM05 (Jayakumar et al., 2021).

RSM designs have been efficient tools for evaluating the significant parameters and their interaction impact on the production of biomolecules in bioprocess. The formulations of economic media and optimization strategies for maximum enzyme productivity are enormously necessary for scale up levels in industries. Our results suggest controlled concentrations of glucose, CASP, casein and mustard oil cake for maximum subtilisin yield as excess substrates are known to affect the microbial growth and interfere with the metabolic aspects of the organism thereby producing lower yields. Several researchers have studied the interactions of factors influencing the production. The protease production by *Shewanella algae* was optimized by Box-Behnken (BB) factorial design for factors like pH, temperature, gelatin and Beef extract (Javee et al., 2022). A central composite rotatable design and artificial neural network optimization gave a 2.2-fold enhancement in mutant kGy-04-UV-25 (Asitok et al., 2022). CCD-RSM model was employed for protease optimization in mutant of *B. subtilis* strain (Shafique

et al., 2021). A 1.3-fold in alkaline protease activity was obtained by BB design in *B. cereus* KM05 (Jayakumar et al., 2021). Elyasi Far et al. (2020) reported an optimum level of glucose and soybean protein to be 0.5 g/L and 38 g/L respectively to enhance production. Optimization of wheat bran was found to produce maximum protease using BB method by *Streptomyces* sp. GS – 1 (Sarkar and K, 2020). A milk clotting enzyme was optimized with 2.3 folds improvement by CCD in *B. subtilis* subsp. *subtilis* strain 168 (Wehaidy et al., 2020). BBD was used by Özbek Yazıcı and Özmen (2020) to optimize the parameters for the collaborative production of proteases and cellulose.

The maximum amount of haloalkaline serine protease from a haloalkaliphilic archaeon *Natrialba hulunbeirensis* strain WNHS14 produced after treatment at 40 °C and pH 9 with a 6-fold increase in yield was 62.9 U/mL owing to the Box-Behnken design, which concentrated the most effective concentrations of the three significant variables casamino acids, KCl and NaCl (Ahmed et al., 2021). Enzymatic effectiveness in agitated containers was significantly enhanced by multiple magnitudes through computational modelling like two-level factorial design (2-LFD) to screen significant factors and the decision was made to employ a central composite rotatable design (CCRD) matrix from the realm of surface methodology (RSM) in order to ascertain the optimal quantity of elements. The forecast of the optimal concentrations of the independent factors leading to maximum thermostable haloalkaline protease production was achieved using an Artificial Neural Network (ANN) technique (Asitok et al., 2022). Optimizing factors to achieve higher yields of the desired product involves the implementation of a proficient and rational statistical approach. The Taguchi $L_8(2)^4$ design was adopted to figure out the best combinations of screening parameters to enhance the production of biosurfactant. This technique makes it feasible to establish the comparative significance and percentage involvement of different variables to maximize the manufacturing of a product (Kumari et al., 2023).

The kinetics profile of subtilisin production in the present study indicated maximum production of subtilisin and protein occurred on the 3rd d. The organism immediately uses glucose as a major carbon source as an alternative source of energy to manufacture a variety of metabolites during the growth phase. The consumption of glucose is evidenced throughout the fermentation period and is negatively associated with cell growth and enzyme production. The increase in cell biomass represents the consumption of nutrients available in the medium to trigger enzyme and metabolite expression. The synthesis of products usually declines in death phase. The enzyme production usually declines after a specific time period possibly due to the process of protein denaturation or degradation. Subtilisin enzyme is a primary metabolite and growth associated. Diverse fermentation profiles are reports with specific strains in the literature. Protease production was highest on 5th d and decreased after 6th d in *Streptomyces* sp. Al-Dhabi-82 (Abdullah Al-Dhabi et al., 2020). The alkaline protease production was maximum after 24 h in case of *B. subtilis* AKAL7 and *Exiguobacterium indicum* (Hakim et al., 2018). Several models of kinetics such as, Luderking-Piret, Monod and Gompertz models are studied in the literature for protease production (Asitok et al., 2022). The kinetics study in 5 L bioreactor from a mutant strain kGy-04-UV-25 depicted the biomass formation developed after 5 h and substrate was utilized and directed for cellular metabolism (Asitok et al., 2022). In related research, serine protease production by *Paenibacillus graminis* MC 2213 by fermentation process yielded maximum activity at 96 h with 15.9 U/mL activity (Couto et al., 2022). According to the production kinetics, designing a medium with abundant nutritional sources boosts enzyme productivity.

The current work shows that subtilisin-capped silver and zinc oxide nanoparticles have been successfully synthesized. Multiple researchers have documented the alteration in suspension color

as an indicative sign of nanoparticle synthesis (Sidhu and Nehra, 2021). Literature reports have documented for the biological synthesis of AgNP using various *Bacilli* species, including *B. licheniformis*, *Lysinibacillus sphaericus*, *B. subtilis*, *B. thuringiensis*, *B. cereus*, *B. pumilus*, *B. brevis*, *B. marisflavi*, *B. amyloliquefaciens*, *B. flexus*, *B. megaterium*, and *B. methylotropicus* (El-Bendary et al., 2021). The optical characteristics of biologically generated silver nanoparticles (AgNP) were investigated using UV-vis spectroscopy, which is dependent on the size and form of the nanoparticles. The synthesis carried out under optimized conditions led to a notable increase in absorbance, accompanied by the emergence of a distinct and intense peak at 432 nm of Bac23-capped silver nanoparticles extracted from *Lactobacillus plantarum* (Sidhu and Nehra, 2021). In another study, after 24 h of incubation, the formation of AgNP was evidenced by absorption peaks at 405 nm and 420 nm for *Bacillus amyloliquefaciens* and *B. subtilis* respectively, to investigate the harmful effect on *Cx. Pipiens* larvae and pupae (Fouad et al., 2017). A similar study of subtilisin conjugated AuAgNP depicted a narrow peak at 564 nm by UV-Vis spectroscopy. While the bi-metallic nanoparticles formed without subtilisin showed characteristic bands at 513 nm and 318 nm for gold and silver respectively. This shift depicts that the nanoparticle structure does influence the biocatalytic activity. The covalent attachment of proteins to the surface of Au/Ag core-shell nanoparticles is essential for their biological functionality and biocompatibility, allowing for tailored interactions with biological systems and enabling specific applications in biomedicine and bioengineering (Prabhawathi et al., 2019). Other results were broadly in-line with the present findings stating that UV-Visible spectroscopy was performed to identify the presence of lipopeptides (secondary metabolite of *B. subtilis* SDUM301120) on the surface of AgNP. The absorption spectra depicted the peaks ranging between 430 and 460 nm which was more specific and proved to be enhancing the antibacterial efficiency (Yu et al., 2021). A characteristic peak of ZnONP from *P. austroarabica* extract was at 362 nm indicating the formation of nanoparticles. After 4 h of incubation, the solution's absorbance increased partially. However, the color of the solution was unchanged and the degree of absorption maintained steady after 24 h. These findings imply that the solution's Zn^{2+} ion reduction was thorough. The stabilization of absorbance over time suggests that the reaction reached its endpoint, and the reduction of Zn^{2+} ions to zinc nanoparticles (ZnNP) was successfully achieved (Alahdal et al., 2022). Another study looked at the green manufacture of zinc nanoparticles to see how they affected the yield and growth of *Pisum sativum* L. A sharp peak at 374 nm was observed which indicates the formation of white colored nanoparticles (Ahmed et al., 2022). This is consistent and in-line to our study with what has been found recently in characterizing the green-synthesized ZnONP having an absorption peak wavelength at 384 nm using the aqueous extracts of *Cassia siamea* (L.). Zinc oxide nanoparticles (ZnO-NP) possess exceptional catalytic efficiency and exhibit a strong adsorption capacity. As a result, they are becoming increasingly utilized in the manufacturing of sunscreens. They are also efficient against bacteria that are resistant to antibiotics (Ahmad Khan et al., 2023). Various kinds of nanoparticles have been employed to study its characteristics. In a related work, an easy and inexpensive technique for producing selenium nanoparticles (SeNPs) employing probiotic *B. subtilis* BSN313 was developed. By virtue of the substantial surface-to-volume ratio, elevated surface energy, spatial confinement, and decreased defects, SeNPs exhibit exceptional physical and chemical attributes (Ullah et al., 2021). A study reported by Hosseini-Koupaei et al. (2019), investigated the interactions and stability of proteinase K, a subtilisin-like serine protease in the presence of copper oxide (CuO) nanoparticles, with broad implications in the realms of biology, medicine, and commercial uses. The primary

aims were to assess the impact of CuO nanoparticles on the functionality, robustness, and configuration of proteinase K as a representative enzyme, employing diverse spectroscopic methods. The nanoparticles are safe and compatible with living organisms, exhibiting remarkable medical uses such as fighting cancer (anti-cancer), reducing inflammation (anti-inflammatory), and combating microbes (antimicrobial). These particles also excel in specific drug transport, promoting healing of wounds, and advanced biological imaging. A study reported, samples containing zinc oxide nanoparticles prepared by aqueous fruit extracts of *Myristica fragrans* were tested for their ability to inhibit α -amylase and α -glucosidase enzymes. It reveals the remarkable antidiabetic properties of biobased nanoparticles. They emerge as a promising therapeutic solution for diabetes treatment, presenting a cost-effective and more efficient alternative to conventional drugs. Different concentrations of biogenic ZnO-NPs were tested for antileishmanial activity against amastigotes and promastigotes (Faisal et al., 2021). Another research reveals the *in vitro* assessment of the anti-inflammatory potential of $TiO_2@ZnO$ -Au nanostructures. This was accomplished by studying their ability to inhibit protein denaturation, a key indicator of anti-inflammatory activity. Protein denaturation happens as a result of injury to tissues following inflammation and rheumatic responses. Suppressing protein denaturation represents a significant mechanism by which NSAIDs act in situations involving inflammation, such as rheumatic conditions (Pragathiswaran et al., 2020). Nanoparticle size plays a crucial role in antimicrobial activity. Small-sized nanoparticles can penetrate into microbial cell membranes more easily, leading to enhanced antimicrobial effects. Additionally, nanoparticles with larger surface areas provide more contact points for interaction with microorganisms, boosting their antimicrobial efficacy. Nanoparticles can exhibit synergistic effects when combined with traditional antimicrobial agents or other nanoparticles. Such combinations can enhance antimicrobial activity and help overcome microbial resistance. Subtilisin and its capped nanoparticles have shown excellent antibacterial activity at higher concentrations against both Gram-positive as well as Gram-negative pathogens with the lowest MICs. The antimicrobial activity of *B. subtilis* cell-supernatant used for biogenic silver nanoparticles against multi-drug resistance microbes was studied in which the maximum inhibition was seen for *Klebsiella pneumoniae* followed by *E. coli*. This coincides with our results of *E. coli* showing the highest inhibition from our study. The lowest MIC (300 μ g/mL) was shown for *Klebsiella pneumoniae* (Alsamhary, 2020). In another study, the synthesized *Bacillus mn14*-AgNPs (Bs-AgNPs) has shown 20 mm and 18 mm inhibition zone against *S. viridans* and *S. Aureus* respectively, larger than the positive control tetracycline (17 mm) (Kabeerdass et al., 2021). Previous studies have reported that *Bacillus megaterium* silver nanoparticles exhibited significant antimicrobial activity against various pathogens, including *P. aeruginosa*, *S. typhi*, *Proteus vulgaris*, *Streptococcus pneumoniae*, *S. aureus* and *E. coli*. The silver nanoparticles derived from *Bacillus methylotrophicus* demonstrated antimicrobial activity against several pathogens, including *Candida albicans*, *E. coli*, *Salmonella enterica*, and *Vibrio parahaemolyticus* (El-Bendary et al., 2021). The conjugation of AuAgNP (gold-silver nanoparticles) with subtilisin has enhanced its activity against *S. aureus*, resulting in an increased antimicrobial efficacy. However, this conjugation has the opposite effect on its activity against *E. coli*, where the antimicrobial activity is reduced (Prabhawathi et al., 2019). The current study's findings demonstrate that the antimicrobial effectiveness of nanoparticles (NPs) with increased antibacterial qualities is not just the sum of the individual impacts of pure NPs and subtilisin, instead, it shows a synergistic interaction between the two, resulting in NPs with improved antibacterial capabilities and a more effective antimicrobial potential. The precise mechanism behind the antibacterial

behaviour of nanoparticles is not entirely known. However, it has been reported that the overproduction of ROS is considered a primary mechanism of nanoparticle toxicity and cell damage. ROS, including free radicals such as superoxide anions (O_2^-), hydrogen peroxide (H_2O_2) and hydroxyl radicals (OH^-) can induce oxidative stress within bacterial cells, leading to cellular damage, membrane disruption, DNA damage and ultimately cell death. While excessive ROS generation is known to contribute to nanoparticle antibacterial effects, it is crucial to stress that a thorough knowledge of the processes involved requires more research and analysis. The damage inflicted upon cellular components and the dysregulation of calcium homeostasis caused by ROS contribute to the induction of bacterial apoptosis in the presence of AgNPs (Yu et al., 2021). The phytochemically synthesized ZnO@Cs-NPs revealed inhibition against infectious strains *P. aeruginosa* PAO1 and *C. Violaceum* with an inhibition zone of 20 mm and 15 mm respectively and MIC values were found to be 80 and 60 $\mu\text{g}/\text{mL}$ respectively. The enhanced antibacterial activity of ZnO@Cs-NPs is believed to stem from their larger surface area, which enables greater interaction with microbes. The literature highlights the significant contribution of synergistic interactions between the particles and natural chemicals in the observed augmentation of antibacterial activity exhibited by ZnO@Cs-NPs (Ahmad Khan et al., 2023). However, there are very few studies reported on antibacterial efficiency of subtilisin-capped zinc oxide nanoparticles from *B. subtilis* which is presented in the current study.

Recently, many other nanoparticles have shown several biological activities like, varied concentrations of $TiO_2@ZnO$ -Au nanocomposites have been demonstrated to be the most efficient over test organisms *E. coli* and *S. aureus*, reason being the production of ROS as an antibacterial mechanism resulting in cell related degradations (Pragathiswaran et al., 2020).

Antioxidants in nanoparticles serve a vital purpose in protecting cellular structures and tissues from oxidative stress caused by reactive oxygen species (ROS). Oxidative stress is linked to a variety of illnesses and signs of aging. Antioxidant nanoparticles can scavenge ROS, neutralize free radicals, and prevent cellular damage. Antioxidant nanoparticles have the ability to improve the effectiveness of drugs by safeguarding them against degradation or inactivation caused by oxidation. When drugs are encapsulated within antioxidant nanoparticles, their stability and availability within the body can be enhanced, resulting in improved therapeutic results. Previous research has found similar outcomes to ours indicating antioxidant activity of 67.4% and 51.02% for biologically-synthesized AgNP and chemically-synthesized AgNP with DPPH scavenging assay. Silver nanoparticles are renowned for their remarkable catalytic activity in specific oxidation reactions, such as CO oxidation. In contrast, bulk silver metal exhibits limited chemical reactivity due to its compact size and the nature of its interactions. The unique size-dependent properties of silver nanoparticles contribute to their enhanced catalytic performance, making them highly effective catalysts in various oxidation processes. Based on this knowledge, organically generated silver nanoparticles may cause an increase in the generation of oxygen species that are reactive (ROS), resulting in oxidative stress. The unique properties of silver nanoparticles may contribute to their ability to generate ROS, leading to potential oxidative damage to biological systems. This leads to damaging the proteins and nucleic acids thereby causing apoptosis or death of the cell (Chojniak-Gronek et al., 2022). Another research showed, at 100 $\mu\text{g}/\text{mL}$, green synthesis of AgNPs with aqueous extract of *Aquilegia pubiflora* leaves had the following DPPH and ABTS free radical scavenging activity, with $51.28 \pm 0.94\%$ and TEAC (Trolox equivalent antioxidant capacity) value of 63.73 ± 0.95 respectively along with few other assays like total reduction power (TRP) and total antioxidant capacity (TAC) (Jan et al., 2021). Another work presented by

(Ibrahim et al. (2021), investigated the optimization of silver nanoparticles with *B. cereus*. Its free radical scavenging activity with DPPH and anti-radical activity with ABTS at varying time intervals between 16 and 40 min. was found to be maximum. The DPPH activity was significant at 94.01% post incubation of 30 min. The purple color observed during the reaction faded upon reduction, indicating the presence of antioxidant activity in the added sample. In relation to our study of ZnONP, DPPH scavenging showed maximum activity of 65.5% at 100 $\mu\text{g}/\text{mL}$ concentration for biocompatible AgNPs synthesized by endophytic *B. cereus* (MT193718) isolated from *Berberis lyceum*. The fact that the inhibition percentage of AgNPs was extremely close to that of ZnONPs activity indicates that the principle of working of nanoparticles is comparable (Mujaddidi et al., 2021). Another study exhibited the characteristics of purified antimicrobial peptide called subtilisin from *B. firmus* VE2, showing dose-dependent DPPH scavenging of $96.5 \pm 0.56\%$ at 50 $\mu\text{L}/\text{mL}$ (Manikandan et al., 2021). This result ties well with previous studies wherein, increase in the concentration of ZnONPs thereby increased the DPPH scavenging activity showing highest inhibition of 85.17% in comparison to the *P. austroarabica* extract and ascorbic acid (Alahdal et al., 2022). The above stated study matches with the findings from our study with respect to subtilisin-capped ZnONP acting as a potential antioxidant agent to provide protection from oxidative stress. Antioxidant nanoparticles find applications in various biomedical fields, including drug delivery systems, imaging agents, tissue engineering, and regenerative medicine. Their antioxidant properties enhance biocompatibility, reduce cytotoxicity, and improve overall performance in these applications.

The MTT assay provides quantitative results, allowing for the comparison of different compounds and their respective cytotoxic effects on various cancer cells. This enables researchers to rank the efficacy of potential anticancer agents. The assay is frequently used as a primary screening tool to identify potential anticancer candidates. Compounds that show significant cytotoxic effects in the MTT assay can be further investigated in more complex *in vivo* models. Additional studies may be required to elucidate the precise mechanisms of action. Our studies have shown potential anticancer activity with less IC_{50} value proving it to be inhibiting the cancerous cell lines at 50%. Both nanoparticles can be treated as effective anticancer agents. The findings align with previous reports suggesting that biosynthesized silver nanoparticles demonstrate significant efficacy in their actions at 30 $\mu\text{L}/\text{mL}$ or higher. The observed activity could be ascribed to AgNP's synergistic impact and also bioactive compounds, such as biosurfactants, that adhere to the surfaces of the nanoparticles. This combination of AgNP and bioactive compounds may contribute to the enhanced overall effectiveness of the nanoparticles in the observed activity. To further validate these results and their potential therapeutic applications, additional studies using *in vivo* models are necessary. *In vivo* investigations will give a more full knowledge of nanoparticle behavior and effectiveness within living beings, laying the foundation for their future translation to clinical applications (Chojniak-Gronek et al., 2022). The cytotoxic effects of biosynthesized AgNPs utilizing *B. subtilis* extracellular filtrate on lung carcinoma (A549), liver carcinoma (HepG-2) and African green monkey kidney epithelial (MA104) cell lines were investigated. The CC_{50} values for these cell lines were found to be 212.5 mg/mL , 6.4 mg/mL and 78.9 mg/mL respectively. These values represent the concentration of the AgNPs that caused 50% cytotoxicity in each cell line (El-Bendary et al., 2021). Numerous reports have highlighted the harmful effects of AgNPs on cancer cells. Mukherjee & Nethi, (2019) also that silver nanoparticles have been shown to have anticancer action against a variety of cancer cell types. These findings demonstrate the potential of AgNPs as a promising candidate for cancer therapy and warrant further investigation in this area. The

mechanistic pathway of nanoparticle-induced cytotoxicity is often mediated by the repeated generation of intracellular oxidative stress. This process of oxidative stress overwhelms the cellular antioxidant defense systems, causing components of the cell, including DNA, to be damaged. As a consequence, apoptosis is triggered in cancer cell lines, leading to programmed cell death. This cascade of events highlights the potential of nanoparticles as agents for inducing targeted cell death in cancer therapy. More study is needed to completely comprehend the intricate mechanisms that underpin nanoparticle-induced cytotoxicity and mortality in cancer cells. The biosynthesized GST-AgNPs (*Gloriosa superba* L. tuber extract-capped silver nanoparticles) exhibited 65.08% viability at 60 $\mu\text{g/mL}$ in lung cancer cells of A549 (Murugesan et al., 2021). In our study, we also found that Ag-NPs are capable of inducing oxidative stress by generating reactive oxygen species (ROS). These ROS possess the ability to harm DNA, leading to the mortality of cancerous cells. This observation suggests that the mechanism of action of Ag-NPs in inhibiting cancer cell growth involves ROS-mediated oxidative damage, which further supports their potential as a therapeutic option in cancer treatment (Jan et al., 2021). Recombinant subtilisin has also demonstrated promising anticancer activity against breast cancer cell lines (Shettar et al., 2023). Therefore, in the current study, nanoparticles have proven to be potential to multiple biological activities like antibacterial, antioxidant and anticancer agents.

Recently, a study showed dose dependent cytotoxic activity found in the Brazilian Red Propolis (BRP) extract (a bee product), and biosynthesized gold nanoparticles (AuNPs) were evaluated in bladder cancer cells (T24) derived from transitional cell carcinoma grade II and prostate cancer cells (PC-3) derived from bone metastasis from grade IV adenocarcinoma. These observations could potentially be elucidated through an exploration of the gold nanoparticle fabrication process, where samples were employed to reduce Au^{3+} ions, leading to the generation of metallic nanoparticles (Botteon et al., 2021). Another work employed a sustainable approach (green synthesis) for producing silver nanoparticles using a water-based extract derived from pomegranate leaves (*Punica granatum*). The study aimed to explore the potential anticancer effects of these nanoparticles on human cervical cancer cells (HeLa) with a dose-response curve to induce apoptosis (Sarkar and Kotteeswaran, 2018).

The FTIR spectrum of subtilisin-capped silver and zinc oxide nanoparticles revealed the presence of numerous groups with functional properties, according to current study, including C–O and C–N stretching in amides, OH and NH_2 groups, C–H stretching and C–C stretch of alkynes. These characteristic absorption bands offer valuable information about the molecular composition and structure of the biosynthesized nanoparticles, providing insights into the biomolecules involved in the synthesis process. This information is essential for understanding the unique properties and potential applications of the synthesized nanoparticles. Similar vibrations and peaks have been found in several studies. The results show that hydroxyl (OH) groups, C–C–O groups, and amide chains are the key functional groups implicated in the reduction and persistence of Bac23-capped SNPs. These results strongly suggest that the bacteriocin protein likely demonstrated a vital role in both the synthesis and capping of the nanoparticles (Sidhu and Nehra, 2021). The large stretch of 3394 cm^{-1} from the present study coincides with the absorption peak at 3308 cm^{-1} indicating the presence of amide bands and N–H mode from AuAgNP coated with subtilisin molecule (Prabhawathi et al., 2019). The characteristic spectra of AgNPs were reported using a supernatant free of cells of *B. amyloliquefaciens* (D29). The robust interaction between water and the AgNP surface is likely accountable for the O–H stretching and the occurrence of functional groups such as C = C, C–H, C = O, and N–H. These functional structures

might be associated with residues of amino acids and protein molecules engaged in the microbiological production of AgNPs. The strong associations between water molecules and the nanoparticles are presumed to have a vital role in stabilizing and facilitating the bonding of biomolecules on the AgNP surfaces during the synthesis process. Distinctive peaks with minor shifts were also seen in AgNPs by *B. subtilis* (A15) in the same study (Fouad et al., 2017). Another study on formation of zinc oxide nanoparticles biosynthesized from *P. austroarabica* extract showed similar peaks and play a substantial role the reduction of Zn ions and function as capping agents for ZnONPs (Alahdal et al., 2022). The identification of amino acid peaks in the clear filtrate verifies the existence of proteins in the material being studied, determined by the UV–vis spectra. FTIR spectra were utilized to distinguish potential relationships between silver and bio-active substances that might be liable for the formation and endurance of silver nanoparticles as a protective coating (Alsamhary, 2020).

From the SEM-EDS results of subtilisin-capped Ag and ZnO nanoparticles, this study confirms the appearance and elemental composition of the nanoparticles formed with respect to the studies performed by many other researchers. In a similar study, a prominent peak at 3 keV indicates abundance in silver in nanoparticles formed from strawberry fruit pomace extract with 53.29% weight of Ag. This exactly is in line with the results of current research (Alam, 2022). The micrograph images of freeze-dried AgNP from *B. amyloliquefaciens* and *B. subtilis* were spherical in nature and the EDS pattern showed Ag at 3 keV (Fouad et al., 2017). SEM morphology of mesoporous silica nanoparticles of subtilisin showed spherical nanoparticles with size ranging from 60 to 100 nm (Özbek and Ünal, 2017). Jeyabharathi et al. (2022) showed that biological synthesis of ZnO nanoparticles from the leaf extract of *Wattakavolubilis* revealed homogenous distribution. It was also confirmed by EDX spectrum that the nanoparticles contained high amount of Zn and O. Studies showed that the ZnONP were highly compatible having excellent antibacterial and anti-diabetic activities. Similar results were also seen from the zinc nanoparticles synthesized using *P. austroarabica* which revealed the existence of metals in it and presence of carbon illustrates that plant phytochemicals are involved in the reduction and capping of biosynthesized ZnONPs (Alahdal et al., 2022).

The current research on the thermal stability of both silver and zinc oxide nanoparticles conjugated with subtilisin has shown its stability up to $\sim 900\text{ }^\circ\text{C}$. In a related study, the thermal stability of biosynthesized AgNP produced from the extract of strawberry fruit pomace was evaluated using TGA under a nitrogen atmosphere. Up to 75% by weight with stability was possessed by the AgNP (Alam, 2022). These results are very much similar to the findings from the current study of subtilisin-capped AgNP. Chitosan polymer-coated mesoporous silica nanoparticles showed a weight loss of 28.8% while the pure polymer depicted a weight loss of 68.9% (Özbek and Ünal, 2017). The decrease in weight was up to 60% between 300 and 400 $^\circ\text{C}$ and resulted due to decomposition of organic components. The green production of AgNP utilizing *Aquilegia pubiflora* leaves was reported by Jan et al. (2021). Bacterial cellulose derived from the thermophilic *B. licheniformis* species demonstrated excellent heat stability up to 250 $^\circ\text{C}$ (Bagewadi et al., 2020b). From the findings of similar nanoparticles studies reported by other researchers, it states that subtilisin-capped nanoparticles have good thermal stability and these findings are less reported.

The results from the current study of subtilisin-capped AgNP and ZnONP revealed spherical and rough morphology which have been similarly reported by other research works in literature. AFM images of AgNP synthesized from the extracts of Marine seaweed *Gelidiallacerosa* was studied for its morphology and appeared to be showing agglomeration clearly (Thiruchelvi et al., 2021). The filtrate of *Trichoderma harzianum* was used to

investigate the importance of capped and uncapped AgNP. AFM pictures of uncapped nanoparticles revealed large mean diameters, whilst capped nanoparticles were discovered to be circular in form (Guilger-Casagrande et al., 2021). The average particle size of eco-friendly ZnONP from *Cymodocea serrulate* showed 47 nm with similar morphology reported as others (Rajeswaran et al., 2019). In a related study, the images of zinc oxide nanoparticles from *B. subtilis* illustrated the roughness on the surface with uniform distribution (Fazaa, 2022). In comparison to the current research, biogenic ZnONP biosynthesized from *B. subtilis* revealed rough outermost surface with approximately 65.17 nm average diameter.

XRD analysis allows researchers to confirm the crystallinity and purity of the nanoparticles, as well as gain insights into their size, shape and composition. It is a widely used method for characterizing nanoparticles in materials science, nanotechnology and various research fields. The XRD pattern of AgNP and ZnONP from the current research shows crystalline structure and the diffraction peaks matches with the cubic lattices. In a related study, ZnONP with lipase immobilization has depicted crystalline nature and showed similar 2θ values (Khan et al., 2019). Zinc acetate was employed as a substrate in the fabrication of ZnO nanoparticles using extracts of *Wattakaka volubilis*, which showed amorphous nature with average particle size of 16.79 nm (Jeyabharathi et al., 2022). The strong intensity of the Bragg reflections in the XRD spectrum reveals an appearance of robust X-ray dispersion sites within crystallized state of the nanoparticles. This high intensity could be attributed to proteins that were available in the nanoparticles during the synthesis process. These proteins may have contributed to the formation and stabilization of the crystalline structure of the nanoparticles, leading to the distinct X-ray scattering pattern observed in the diffractogram. The involvement of proteins in the synthesis process highlights their potential role in shaping the properties and structure of the nanoparticles. In this case it states that subtilisin contributes to the formation of nanoparticle crystals which is more evident (Omole et al., 2018). The reduced particle size and enormous number of crystalline planes in the produced nanoparticles are responsible for the widening observed in all of the peaks. The reduction in intensity in the diffraction patterns of nanoparticles is caused by the broadening of peaks. As nanoparticles have smaller sizes compared to bulk materials, their crystal grains become smaller and more numerous, leading to an increased number of crystallographic planes exposed on the particle surfaces. The peak broadening and reduced intensity are typical characteristics of nanocrystalline materials and provide valuable information about the size and crystallinity of the nanoparticles (Upadhyay et al., 2020). The scarcity of studies focusing on subtilisin-capped AgNP and ZnONP adds novelty to our current work. The limited research in this specific area indicates that our study can contribute valuable insights and unique findings regarding the production, evaluation, analysis and prospective implementations of these nanomaterials.

5. Conclusion

Subtilisin production was evaluated using agro-wastes such as, custard apple seed powder and mustard oil cake from isolated *Bacillus subtilis* strain ZK3. The implementation of Plackett-Burmann (screening design) and response surface methodology (optimization design) revealed a 7.67 folds enhancement. The kinetics profile depicts the maximum production of 77 U/mL on 3rd d. The synthesized subtilisin capped silver and zinc oxide nanoparticles demonstrated biological properties such as, antibacterial, antioxidant and cytotoxic activities. Structural, surface and functional characterizations of nanoparticles showed its thermostable nature. The study provides insights into the applications

of subtilisin and its nanoparticles for promising biological functions.

Author contributions

SS and ZB designed the study concept. SS and HK conducted the experimental studies related to optimization, nanoparticle synthesis and biological properties. SS, ZB and HK carried out analytical studies, interpretations and elucidation of data. SS and ZB have drafted the entire manuscript. TY and SM provided critical reviews and valuable suggestions on the structure of manuscript. All the authors have given their consent and agreed to the contents of the manuscript. ZB has been involved in the overall supervision of the research work conducted and contributed in resource management.

Declaration of Competing Interest

The authors declare that they have no known competing financial interests or personal relationships that could have appeared to influence the work reported in this paper.

Acknowledgements

The authors are pleased to express their gratitude to the Dean-ship of Scientific Research at King Khalid University for funding this investigation through a small group research project with the grant number R.G. P. 1/123/44.

Appendix A. Supplementary data

Supplementary data to this article can be found online at <https://doi.org/10.1016/j.sjbs.2023.103807>.

References

- Abdullah Al-Dhabi, N., Ali Esmail, G., Mohammed Ghilan, A.-K., Valan Arasu, M., Duraipandian, V., Ponmurugan, K., 2020. Characterization and fermentation optimization of novel thermo stable alkaline protease from *Streptomyces* sp. Al-Dhabi-82 from the Saudi Arabian environment for eco-friendly and industrial applications. *J. King Saud Univ. - Sci.* 32, 1258–1264. <https://doi.org/10.1016/j.jksus.2019.11.011>.
- Adetunji, A.I., Olaniran, A.O., 2020. Statistical modelling and optimization of protease production by an autochthonous *Bacillus aryabhatai* Ab15-ES: A response surface methodology approach. *Biocatal. Agric. Biotechnol.* 24, <https://doi.org/10.1016/j.cbab.2020.101528> 101528.
- Ahamad Khan, M., Lone, S.A., Shahid, M., Zeyad, M.T., Syed, A., Ehtram, A., Elgorban, A.M., Verma, M., Danish, M., 2023. Phylogenically synthesized zinc oxide nanoparticles (ZnO-NPs) potentially inhibit the bacterial pathogens. *In Vitro Studies. Toxics* 11, 452. <https://doi.org/10.3390/toxics11050452>.
- Ahmed, R.S., Embaby, A.M., Hassan, M., Soliman, N.A., Abdel-Fattah, Y.R., 2021. Optimization, purification, and characterization of haloalkaline serine protease from a haloalkaliphilic archaeon *natrialba hulunbeirensis* strain WNHS14. *Microbiol. Biotechnol. Lett.* 49, 181–191. [10.48022/mbi.1904.04003](https://doi.org/10.48022/mbi.1904.04003).
- Ahmed, S., Qasim, S., Ansari, M., Shah, A.A., Rehman, H.U., Shah, M.N., Ghafoor, U., Naqvi, S.A.H., Hassan, M.Z., Rehman, S. ur, Ahmad, F., Shoaib, S., Alahmadi, T.A., Alharbi, S.A., Datta, R., 2022. Green synthesis of zinc nanoparticles and their effects on growth and yield of *Pisum sativum*. *J. King Saud Univ. - Sci.* 34, <https://doi.org/10.1016/j.jksus.2022.102132> 102132.
- Alahdal, F.A.M., Qashqoosh, M.T.A., Manea, Y.K., Salem, M.A.S., Khan, A.M.T., Naqvi, S., 2022. Eco-friendly synthesis of zinc oxide nanoparticles as nanosensor, nanocatalyst and antioxidant agent using leaf extract of *P. australis*. *OpenNano* 8, <https://doi.org/10.1016/j.onano.2022.100067> 100067.
- Alam, M., 2022. Analyses of biosynthesized silver nanoparticles produced from strawberry fruit pomace extracts in terms of biocompatibility, cytotoxicity, antioxidant ability, photodegradation, and in-silico studies. *J. King Saud Univ. - Sci.* 34, <https://doi.org/10.1016/j.jksus.2022.102327> 102327.
- Alfarouk, K.O., Stock, C.-M., Taylor, S., Walsh, M., Muddathir, A.K., Verduzco, D., Bashir, A.H.H., Mohammed, O.Y., Elhassan, G.O., Harguindey, S., Reshkin, S.J., Ibrahim, M.E., Rauch, C., 2015. Resistance to cancer chemotherapy: failure in drug response from ADME to P-gp. *Cancer Cell Int.* 15, <https://doi.org/10.1186/s12935-015-0221-1> 71.
- Alsamhary, K.I., 2020. Eco-friendly synthesis of silver nanoparticles by *Bacillus subtilis* and their antibacterial activity. *Saudi J. Biol.* 27, 2185–2191. <https://doi.org/10.1016/j.sjbs.2020.04.026>.

- Amiri, S., Rezaei Mokarram, R., Sowti Khiabani, M., Rezaezadeh Bari, M., Alizadeh Khaledabad, M., 2022. Characterization of antimicrobial peptides produced by *Lactobacillus acidophilus* LA-5 and *Bifidobacterium lactis* BB-12 and their inhibitory effect against foodborne pathogens. *LWT* 153. <https://doi.org/10.1016/j.lwt.2021.112449> 112449.
- Ashokbhai, J.K., Basaiawmoit, B., Das, S., Sakure, A., Maurya, R., Bishnoi, M., Kondepudi, K.K., Padhi, S., Rai, A.K., Liu, Z., Hatia, S., 2022. Antioxidative, antimicrobial and anti-inflammatory activities and release of ultra-filtered antioxidative and antimicrobial peptides during fermentation of sheep milk: In-vitro, in-silico and molecular interaction studies. *Food Biosci.* 47. <https://doi.org/10.1016/j.fbio.2022.101666> 101666.
- Asitok, A., Ekpenyong, M., Takon, I., Antai, S., Ogarekpe, N., Antigha, R., Edet, P., Ben, U., Akpan, A., Antai, A., Essien, J., 2022. Overproduction of a thermo-stable halo-alkaline protease on agro-waste-based optimized medium through alternate combinatorial random mutagenesis of *Stenotrophomonas acidaminiphila*. *Biotechnol. Reports* 35, e00746.
- Azrin, N.A.M., Ali, M.S.M., Rahman, R.N.Z.R.A., Oslan, S.N., Noor, N.D.M., 2022. Versatility of subtilisin: A review on structure, characteristics, and applications. *Biotechnol. Appl. Biochem.* 69, 2599–2616. <https://doi.org/10.1002/bab.2309>.
- Bagewadi, Z.K., Mulla, S.I., Nannekar, H.Z., 2016. Purification and characterization of endo β -1,4-d-glucanase from *Trichoderma harzianum* strain HZN11 and its application in production of bioethanol from sweet sorghum bagasse. 3. *Biotech* 6. <https://doi.org/10.1007/s13205-016-0421-y> 101.
- Bagewadi, Z.K., Mulla, S.I., Nannekar, H.Z., 2017a. Purification and immobilization of laccase from *Trichoderma harzianum* strain HZN10 and its application in dye decolorization. *J. Genet. Eng. Biotechnol.* 15, 139–150. <https://doi.org/10.1016/j.jgeb.2017.01.007>.
- Bagewadi, Z.K., Mulla, S.I., Nannekar, H.Z., 2017b. Optimization of laccase production and its application in delignification of biomass. *Int. J. Recycl. Org. Waste Agric.* 6, 351–365. <https://doi.org/10.1007/s40093-017-0184-4>.
- Bagewadi, Z.K., Mulla, S.I., Nannekar, H.Z., 2018. Optimization of endoglucanase production from *Trichoderma harzianum* strain HZN11 by central composite design under response surface methodology. *Biomass Convers. Biorefinery* 8, 305–316. <https://doi.org/10.1007/s13399-017-0285-3>.
- Bagewadi, Z.K., Muddapur, U.M., Madiwal, S.S., Mulla, S.I., Khan, A., 2019. Biochemical and enzyme inhibitory attributes of methanolic leaf extract of *Datura innoxia* Mill. *Environ. Sustain.* 2, 75–87. <https://doi.org/10.1007/s42398-019-00052-6>.
- Bagewadi, Z.K., Bhavikatti, J.S., Muddapur, U.M., Yaraguppi, D.A., Mulla, S.I., 2020a. Statistical optimization and characterization of bacterial cellulose produced by isolated thermophilic *Bacillus licheniformis* strain ZBT2. *Carbohydr. Res.* 491. <https://doi.org/10.1016/j.carres.2020.107979> 107979.
- Bagewadi, Z.K., Dsouza, V., Mulla, S.I., Deshpande, S.H., Muddapur, U.M., Yaraguppi, D.A., Reddy, V.D., Bhavikatti, J.S., More, S.S., 2020b. Structural and functional characterization of bacterial cellulose from *Enterobacter hormaechei* subsp. *steigerwaltii* strain ZKE7. *Cellul.* 27, 9181–9199. <https://doi.org/10.1007/s10570-020-03412-2>.
- Bagewadi, Z.K., Yaraguppi, D.A., Mulla, S.I., Deshpande, S.H., 2022. Response surface methodology based optimization, partial purification and characterization of alkaline phosphatase isolated from *Pseudomonas asiatica* strain ZKB1 and its application in plant growth promotion. *Mol. Biotechnol.* 64, 984–1002. <https://doi.org/10.1007/s12033-022-00477-1>.
- Balachandran, C., Vishali, A., Nagendran, N.A., Baskar, K., Hashem, A., Abd Allah, E.F., 2021. Optimization of protease production from *Bacillus halodurans* under solid state fermentation using agrowastes. *Saudi J. Biol. Sci.* 28, 4263–4269. <https://doi.org/10.1016/j.sjbs.2021.04.069>.
- Benkhar, A., Nadi, Z.J., Badis, A., Rebzani, F., Soraya, B.T., Rekiq, H., Naili, B., Ferradji, F.Z., Bejar, S., Jaouadi, B., 2013. Biochemical and molecular characterization of a thermo- and detergent-stable alkaline serine keratinolytic protease from *Bacillus circulans* strain DZ100 for detergent formulations and feather-biodegradation process. *Int. Biodeter. Biodegr.* 83, 129–138. <https://doi.org/10.1016/j.ibiod.2013.05.014>.
- Botteon, C.E.A., Silva, L.B., Ccana-Capatinta, G.V., Silva, T.S., Ambrosio, S.R., Veneziani, R.C.S., Bastos, J.K., Marcato, P.D., 2021. Biosynthesis and characterization of gold nanoparticles using Brazilian red propolis and evaluation of its antimicrobial and anticancer activities. *Sci. Rep.* 11. <https://doi.org/10.1038/s41598-021-81281-w> 1974.
- Chojniak-Gronek, J.M., Jaiowiecki, Ł., Piazza, G.A., 2022. Bioeffects of silver nanoparticles (AgNPs) synthesized by producer of biosurfactant *Bacillus subtilis* strain: in vitro cytotoxicity, antioxidant properties and metabolic activities of mammalian cells. *Arch. Environ. Prot.* 48, 45–52. <https://doi.org/10.24425/aep.2022.143708>.
- Clerici, N.J., Lermen, A.M., Daroit, D.J., 2021. Agro-industrial by-products as substrates for the production of bacterial protease and antioxidant hydrolysates. *Biocatal. Agric. Biotechnol.* 37. <https://doi.org/10.1016/j.bcab.2021.102174> 102174.
- Couto, M.T.T. do, da Silva, A.V., Sobral, R.V.D.S., Rodrigues, C.H., da Cunha, M.N.C., Leite, A.C.L., Figueiredo, M. do V.B., de Paula Oliveira, J., Costa, R.M.P.B., Conniff, A.E.S., Porto, A.L.F., Nascimento, T.P., 2022. Production, extraction and characterization of a serine protease with fibrinolytic, fibrinogenolytic and thrombolytic activity obtained by *Paenibacillus graminis*. *Process Biochem.* 118, 335–345. <https://doi.org/10.1016/j.procbio.2022.05.005>.
- El-Bendary, M.A., Afifi, S.S., Moharam, M.E., Abo El-Ola, S.M., Salama, A., Omara, E.A., Shaheen, M.N.F., Hamed, A.A., Gawdat, N.A., 2021. Biosynthesis of silver nanoparticles using isolated *Bacillus subtilis*: characterization, antimicrobial activity, cytotoxicity, and their performance as antimicrobial agent for textile materials. *Prep. Biochem. Biotech.* 51, 54–68. <https://doi.org/10.1080/10826068.2020.1789992>.
- Elumalai, P., Lim, J.-M., Park, Y.-J., Cho, M., Shea, P.J., Oh, B.-T., 2020. Agricultural waste materials enhance protease production by *Bacillus subtilis* B22 in submerged fermentation under blue light-emitting diodes. *Bioprocess Biosyst. Eng.* 43, 821–830. <https://doi.org/10.1007/s00449-019-02277-5>.
- Elyasi Far, B., Yari Khosroushahi, A., Dilmaghani, A., 2020. In silico study of alkaline serine protease and production optimization in *Bacillus* sp. Khoz1 closed *Bacillus safensis* isolated from honey. *Int. J. Pept. Res. Ther.* 26, 2241–2251. <https://doi.org/10.1007/s10989-020-10016-8>.
- Faisal, S., Jan, H., Shah, S.A., Shah, S., Khan, A., Akbar, M.T., Rizwan, M., Jan, F., Wajidullah, A.N., Khattak, A., Syed, S., 2021. Green synthesis of zinc oxide (ZnO) nanoparticles using aqueous fruit extracts of myristica fragrans: their characterizations and biological and environmental applications. *ACS Omega* 6, 9709–9722. <https://doi.org/10.1021/acsomega.1c00310>.
- Farooq, S., Nazir, R., Ganai, S.A., Ganai, B.A., 2021. Isolation and characterization of a new cold-active protease from psychrotrophic bacteria of Western Himalayan glacial soil. *Sci. Rep.* 11. <https://doi.org/10.1038/s41598-021-92197-w> 12768.
- Fazaa, S.A., 2022. Eco-friendly synthesis of zinc oxide nanoparticles using *Bacillus Subtilis*, characterization and antibacterial potential against *Staphylococcus aureus* associated with cardiac catheterization. *Iran. J. Catal.* 12, 159–168. <https://doi.org/10.30495/ijc.2022.692257>.
- Fouad, H., Hongjie, L., Yanmei, D., Baoting, Y., El-Shakh, A., Abbas, G., Jianchu, M., 2017. Synthesis and characterization of silver nanoparticles using *Bacillus amyloliquefaciens* and *Bacillus subtilis* to control filarial vector *Culex pipiens pallens* and its antimicrobial activity. *Artif. Cells. Nanomedicine, Biotechnol.* 45, 1369–1378. <https://doi.org/10.1080/21691401.2016.1241793>.
- Guilger-Casagrande, M., Germano-Costa, T., Bilesky-José, N., Pasquato-Stigliani, T., Carvalho, L., Fraceto, L.F., de Lima, R., 2021. Influence of the capping of biogenic silver nanoparticles on their toxicity and mechanism of action towards *Sclerotinia sclerotiorum*. *J. Nanobiotechnology* 19. <https://doi.org/10.1186/s12951-021-00797-5> 53.
- Gulmez, C., Atakisi, O., Dalginli, K.Y., Atakisi, E., 2018. A novel detergent additive: Organic solvent- and thermo-alkaline-stable recombinant subtilisin. *Int. J. Biol. Macromol.* 108, 436–443. <https://doi.org/10.1016/j.ijbiomac.2017.11.133>.
- Hakim, A., Bhuiyan, F.R., Iqbal, A., Emon, T.H., Ahmed, J., Azad, A.K., 2018. Production and partial characterization of dehairing alkaline protease from *Bacillus subtilis* AKAL7 and *Exiguobacterium indicum* AKAL11 by using organic municipal solid wastes. *Heliyon* 4, e00646.
- Hosseini-Koupaei, M., Shareghi, B., Saboury, A.A., Davar, F., Sirotkin, V.A., Hosseini-Koupaei, M.H., Enteshari, Z., 2019. Catalytic activity, structure and stability of proteinase K in the presence of biosynthesized CuO nanoparticles. *Int. J. Biol. Macromol.* 122, 732–744. <https://doi.org/10.1016/j.ijbiomac.2018.11.001>.
- Ibrahim, S., Ahmad, Z., Manzoor, M.Z., Mujahid, M., Faheem, Z., Adnan, A., 2021. Optimization for biogenic microbial synthesis of silver nanoparticles through response surface methodology, characterization, their antimicrobial, antioxidant, and catalytic potential. *Sci. Rep.* 11. <https://doi.org/10.1038/s41598-020-80805-0> 770.
- Jan, H., Zaman, G., Usman, H., Ansir, R., Drouet, S., Gigliolo-Guivarch, N., Hano, C., Abbasi, B.H., 2021. Biogenically proficient synthesis and characterization of silver nanoparticles (Ag-NPs) employing aqueous extract of *Aquilegia pubiflora* along with their in vitro antimicrobial, anti-cancer and other biological applications. *J. Mater. Res. Technol.* 15, 950–968. <https://doi.org/10.1016/j.jmrt.2021.08.048>.
- Javee, A., Malairaj, S., Subramani, N., 2022. Biosynthesis, protease optimization and purification of alkaline serine from *Shewanella algae* and its potential application as silver recovery. *Sustain. Chem. Pharm.* 25. <https://doi.org/10.1016/j.scp.2021.100595> 100595.
- Jayakumar, D., Sachith, S.K., Nathan, V.K., Rishad, K.S.M., 2021. Statistical optimization of the most stable alkaline protease from *Bacillus cereus* KM 05 using response surface methodology. *Biotechnol. Lett.* 43, 2053–2065. <https://doi.org/10.1007/s10529-021-03172-4>.
- Jeyabharathi, S., Naveenkumar, S., Chandramohan, S., Venkateshan, N., Gawwad, M. R.A., Elshikh, M.S., Rasheed, R.A., Al Farraj, D.A., Muthukumar, A., 2022. Biological synthesis of zinc oxide nanoparticles from the plant extract, *Wattakaka volubilis* showed anti-microbial and anti-hyperglycemic effects. *J. King Saud Univ. - Sci.* 34. <https://doi.org/10.1016/j.jksus.2022.101881> 101881.
- Kabeerdass, N., Al Otaibi, A., Rajendran, M., Manikandan, A., Kashmery, H.A., Rahman, M.M., Madhu, P., Khan, A., Asiri, A.M., Mathanmoham, M., 2021. *Bacillus*-mediated silver nanoparticle synthesis and its antagonistic activity against bacterial and fungal pathogens. *Antibiotics* 10. <https://doi.org/10.3390/antibiotics1011334> 1334.
- Kalwasńska, A., Jankiewicz, U., Felföldi, T., Burkowska-But, A., Swiontek Brzezinska, M., 2018. Alkaline and halophilic protease production by *Bacillus luteus* H11 and its potential industrial applications. *Food Technol. Biotechnol.* 56. <https://doi.org/10.17113/ftb.56.04.18.5553>.
- Kandasamy, S., Muthusamy, G., Balakrishnan, S., Duraisamy, S., Thangasamy, S., Seralathan, K.-K., Chinnappan, S., 2016. Optimization of protease production from surface-modified coffee pulp waste and corncobs using *Bacillus* sp. by SSF. *3 Biotech* 6, 167. <https://doi.org/10.1007/s13205-016-0481-z>.
- Khan, M.F., Kundu, D., Hazra, C., Patra, S., 2019. A strategic approach of enzyme engineering by attribute ranking and enzyme immobilization on zinc oxide nanoparticles to attain thermostability in mesophilic *Bacillus subtilis* lipase for detergent formulation. *Int. J. Biol. Macromol.* 136, 66–82. <https://doi.org/10.1016/j.ijbiomac.2019.06.042>.

- Khandia, R., Dadar, M., Munjal, A., Dhama, K., Karthik, K., Tiwari, R., Yattoo, M.I., Iqbal, H.M.N., Singh, K.P., Joshi, S.K., Chaicumpa, W., 2019. A comprehensive review of autophagy and its various roles in infectious, non-infectious, and lifestyle diseases: current knowledge and prospects for disease prevention, novel drug design, and therapy. *Cells* 8, <https://doi.org/10.3390/cells8070674> 674.
- Kumari, K., Behera, H.T., Nayak, P.P., Sinha, A., Nandi, A., Ghosh, A., Saha, U., Suar, M., Panda, P.K., Verma, S.K., Raina, V., 2023. Amelioration of lipopeptide biosurfactants for enhanced antibacterial and biocompatibility through molecular antioxidant property by methoxy and carboxyl moieties. *Biomed. Pharmacother.* 161, <https://doi.org/10.1016/j.biopha.2023.114493> 114493.
- Li, S., Zhu, T., Huang, J., Guo, Q., Chen, G., Lai, Y., 2017. Durable antibacterial and UV-protective Ag/TiO₂@fabrics for sustainable biomedical application. *Int. J. Nanomed.* 12, 2593–2606. <https://doi.org/10.2147/IJN.S132035>.
- Mahmoud, A., Kotb, E., Alqosaibi, A.I., Al-Karmalawy, A.A., Al-Dhuayan, I.S., Alabkari, H., 2021. In vitro and in silico characterization of alkaline serine protease from *Bacillus subtilis* D9 recovered from Saudi Arabia. *Heliyon* 7, e08148.
- Manikandan, P., Moopantakath, J., Imchen, M., Kumavath, R., SenthilKumar, P.K., 2021. Identification of Multi-Potent Protein Subtilisin A from halophilic bacterium *Bacillus firmus* VE2. *Microb. Pathog.* 157, <https://doi.org/10.1016/j.micpath.2021.105007> 105007.
- Matkawala, F., Nighojkar, S., Kumar, A., Nighojkar, A., 2019. Enhanced production of alkaline protease by *Neocosmospora* sp. N1 using custard apple seed powder as inducer and its application for stain removal and dehairing. *Biocatal. Agric. Biotechnol.* 21, <https://doi.org/10.1016/j.bcab.2019.101310> 101310.
- Matkawala, F., Nighojkar, S., Kumar, A., Nighojkar, A., 2021. Microbial alkaline serine proteases: Production, properties and applications. *World J. Microbiol. Biotechnol.* 37, 63. <https://doi.org/10.1007/s11274-021-03036-z>.
- Mba, I.E., Nweze, E.I., 2021. Nanoparticles as therapeutic options for treating multidrug-resistant bacteria: research progress, challenges, and prospects. *World J. Microbiol. Biotechnol.* 37, 108. <https://doi.org/10.1007/s11274-021-03070-x>.
- Mechri, S., Kriaa, M., Berrouina, M.B.E., Omrane Benmrud, M., Zaraï Jaouadi, N., Rekkik, H., Bouacem, K., Bouanane-Darenfed, A., Chebbi, A., Sayadi, S., Chamkha, M., Bejar, S., Jaouadi, B., 2017. Optimized production and characterization of a detergent-stable protease from *Lysinibacillus fusiformis* C250R. *Int. J. Biol. Macromol.* 101, 383–397. <https://doi.org/10.1016/j.ijbiomac.2017.03.051>.
- Mechri, S., Allala, F., Bouacem, K., Hasnaoui, I., Gwaithan, H., Chalbi, T.B., Saaloui, E., Asehraou, A., Noiriél, A., Abousalham, A., Hacene, H., Bouanane-Darenfed, A., Le Roes-Hill, M., Jaouadi, B., 2022. Preparation, characterization, immobilization, and molecular docking analysis of a novel detergent-stable subtilisin-like serine protease from *Streptomyces mutabilis* strain TN-X30. *Int. J. Biol. Macromol.* 222, 1326–1342. <https://doi.org/10.1016/j.ijbiomac.2022.09.161>.
- Modi, A., Raval, I., Doshi, P., Joshi, M., Joshi, C., Patel, A.K., 2023. Heterologous expression of recombinant nattokinase in *Escherichia coli* BL21 (DE3) and media optimization for overproduction of nattokinase using RSM. *Protein Expr. Purif.* 203, <https://doi.org/10.1016/j.pep.2022.106198> 106198.
- Mujaddidi, N., Nisa, S., Al Ayoubi, S., Bibi, Y., Khan, S., Sabir, M., Zia, M., Ahmad, S., Qayyum, A., 2021. Pharmacological properties of biogenically synthesized silver nanoparticles using endophyte *Bacillus cereus* extract of *Berberis lycium* against oxidative stress and pathogenic multidrug-resistant bacteria. *Saudi J. Biol. Sci.* 28, 6432–6440. <https://doi.org/10.1016/j.sjbs.2021.07.009>.
- Mukherjee, S., Nethi, S.K., 2019. Biological synthesis of nanoparticles using bacteria. In: *Nanotechnology for Agriculture*. Springer Singapore, Singapore, pp. 37–51 https://doi.org/10.1007/978-981-32-9370-0_3.
- Murugesan, A.K., Pannerselvam, B., Javee, A., Rajenderan, M., Thiagarajan, D., 2021. Facile green synthesis and characterization of *Gloriosa superba* L. tuber extract-capped silver nanoparticles (GST-AgNPs) and its potential antibacterial and anticancer activities against A549 human cancer cells. *Environ. Nanotechnology, Monit. Manag.* 15, <https://doi.org/10.1016/j.enmm.2021.100460> 100460.
- Naveed, M., Nadeem, F., Mehmood, T., Bilal, M., Anwar, Z., Amjad, F., 2021. Protease—a versatile and ecofriendly biocatalyst with multi-industrial applications: an updated review. *Catal. Lett.* 151, 307–323. <https://doi.org/10.1007/s10562-020-03316-7>.
- Omole, R.K., Torimiro, N., Alayande, S.O., Ajenifuja, E., 2018. Silver nanoparticles synthesized from *Bacillus subtilis* for detection of deterioration in the post-harvest spoilage of fruit. *Sustain. Chem. Pharm.* 10, 33–40. <https://doi.org/10.1016/j.scp.2018.08.005>.
- Özbek, B., Ünal, Ş., 2017. Preparation and characterization of polymer-coated mesoporous silica nanoparticles and their application in Subtilisin immobilization. *Korean J. Chem. Eng.* 34, 1992–2001. <https://doi.org/10.1007/s11814-017-0045-x>.
- Özbek Yazıcı, S., Özmen, I., 2020. Optimization for coproduction of protease and cellulase from *Bacillus subtilis* M-11 by the Box-Behnken design and their detergent compatibility. *Brazilian J. Chem. Eng.* 37, 49–59. <https://doi.org/10.1007/s43153-020-00025-x>.
- Prabhawathi, V., Sivakumar, P.M., Boobalan, T., Manohar, C.M., Doble, M., 2019. Design of antimicrobial polycaprolactam nanocomposite by immobilizing subtilisin conjugated Au/Ag core-shell nanoparticles for biomedical applications. *Mater. Sci. Eng. C* 94, 656–665. <https://doi.org/10.1016/j.msec.2018.10.020>.
- Pragathiswaran, C., Smitha, C., Barabadi, H., Al-Ansari, M.M., Al-Humaid, L.A., Saravanan, M., 2020. TiO₂@ZnO nanocomposites decorated with gold nanoparticles: Synthesis, characterization and their antifungal, antibacterial, anti-inflammatory and anticancer activities. *Inorg. Chem. Commun.* 121, <https://doi.org/10.1016/j.inoche.2020.108210> 108210.
- Rajeswaran, S., Somasundaram Thirugnanasambandan, S., Rengasamy Subramaniam, S., Kandasamy, S., Vilwanathan, R., 2019. Synthesis of eco-friendly facile nano-sized zinc oxide particles using aqueous extract of *Cymodocea serrulata* and its potential biological applications. *Appl. Phys. A* 125, <https://doi.org/10.1007/s00339-019-2404-4> 105.
- Reddy, N., Deekonda, V., Seshagiri, S., Reddy, R., Gangula, A.K., 2022. Production, characterization and applications of proteases produced by *Bacillus licheniformis*, *Acinetobacter pittii* and *Aspergillus niger* using neem seed oil cake as the substrate. *Ind. Crop. Prod.* 187, <https://doi.org/10.1016/j.indcrop.2022.115403> 115403.
- Rozanov, A.S., Shekhovtsov, S.V., Bogacheva, N.V., Pershina, E.G., Ryapolova, A.V., Bytyak, D.S., Peltek, S.E., 2021. Production of subtilisin proteases in bacteria and yeast. *Vavilov J. Genet. Breed.* 25, 125–134 <https://doi.org/10.18699/VJ21.015>.
- Saji, R.S., Prasana, J.C., Muthu, S., George, J., 2021. Experimental and theoretical spectroscopic (FT-IR, FT-Raman, UV-VIS) analysis, natural bonding orbitals and molecular docking studies on 2-bromo-6-methoxynaphthalene: A potential anti-cancer drug. *Heliyon* 7, e07213.
- Salwan, R., Sharma, V., 2019. Trends in extracellular serine proteases of bacteria as detergent bioadditive: alternate and environmental friendly tool for detergent industry. *Arch. Microbiol.* 201, 863–877. <https://doi.org/10.1007/s00203-019-01662-8>.
- Sarkar, G., K. S., 2020. Extraction and characterization of alkaline protease from *Streptomyces* sp. GS-1 and its application as dehairing agent. *Biocatal. Agric. Biotechnol.* 25, <https://doi.org/10.1016/j.bcab.2020.101590> 101590.
- Sarkar, S., Kotteeswaran, V., 2018. Green synthesis of silver nanoparticles from aqueous leaf extract of Pomegranate (*Punica granatum*) and their anticancer activity on human cervical cancer cells. *Adv. Nat. Sci. Nanosci. Nanotechnol.* 9, <https://doi.org/10.1088/2043-6254/aac590> 025014.
- Shafique, T., Shafique, J., Zahid, S., Kazi, M., Alnemer, O., Ahmad, A., 2021. Screening, selection and development of *Bacillus subtilis* apr-IBL04 for hyper production of macromolecule alkaline protease. *Saudi J. Biol. Sci.* 28, 1494–1501. <https://doi.org/10.1016/j.sjbs.2020.11.079>.
- Shankar, A., Kumar, V., Kaushik, N.K., Kumar, A., Malik, V., Singh, D., Singh, B., 2020. Sporotrichum thermophile culture extract-mediated greener synthesis of silver nanoparticles: Eco-friendly functional group transformation and anti-bacterial study. *Curr. Res. Green Sustain. Chem.* 3, <https://doi.org/10.1016/j.crgsc.2020.100029> 100029.
- Sharma, V., Tsai, M.-L., Nargotra, P., Chen, C.-W., Kuo, C.-H., Sun, P.-P., Dong, C.-D., 2022. Agro-industrial food waste as a low-cost substrate for sustainable production of industrial enzymes: a critical review. *Catalysts* 12, <https://doi.org/10.3390/catal12111373> 1373.
- Shettar, S.S., Bagewadi, Z.K., Yaraguppi, D.A., Das, S., Mahanta, N., Singh, S.P., Katti, A., Saikia, D., 2023. Gene expression and molecular characterization of recombinant subtilisin from *Bacillus subtilis* with antibacterial, antioxidant and anticancer properties. *Int. J. Biol. Macromol.* <https://doi.org/10.1016/j.ijbiomac.2023.125960> 125960.
- Sidhu, P.K., Nehra, K., 2021. Purification and characterization of bacteriocin Bac23 extracted from *Lactobacillus plantarum* PKLP5 and its interaction with silver nanoparticles for enhanced antimicrobial spectrum against food-borne pathogens. *LWT* 139, <https://doi.org/10.1016/j.lwt.2020.110546> 110546.
- Talhi, I., Dehimat, L., Jaouani, A., Cherfia, R., Berkani, M., Almomani, F., Vasseghian, Y., Chaouche, N.K., 2022. Optimization of thermostable proteases production under agro-wastes solid-state fermentation by a new thermophilic *Mycothermus thermophilus* isolated from a hydrothermal spring Hammam Debagh. *Algeria. Chemosphere* 286, <https://doi.org/10.1016/j.chemosphere.2021.131479> 131479.
- Taneja, N., Sharma, M., 2019. Antimicrobial resistance in the environment: The Indian scenario. *Indian J. Med. Res.* 149, 119. https://doi.org/10.4103/ijmr.IJMR_331_18.
- Thankappan, B., Sivakumar, J., Asokan, S., Ramasamy, M., Pillai, M.M., Selvakumar, R., Angayarkanni, J., 2021. Dual antimicrobial and anticancer activity of a novel synthetic α -helical antimicrobial peptide. *Eur. J. Pharm. Sci.* 161, <https://doi.org/10.1016/j.ejps.2021.105784> 105784.
- Thebti, W., Riah, Y., Belhadj, O., 2016. Purification and characterization of a new thermostable, haloalkaline, solvent stable, and detergent compatible serine protease from *geobacillus toebii* strain LBT 77. *Biomed Res. Int.* 2016, 1–8. <https://doi.org/10.1155/2016/9178962>.
- Thiruchelvi, R., Jayashree, P., Mirunaalini, K., 2021. Synthesis of silver nanoparticle using marine red seaweed *Gelidium acerosa*—A complete study on its biological activity and its characterisation. *Mater. Today: Proc.* 37, 1693–1698. <https://doi.org/10.1016/j.matpr.2020.07.242>.
- Thomas, N.N., Archana, V., Shibina, S., Edwin, B.T., 2021. Isolation and characterization of a protease from *Bacillus* sps. *Mater. Today: Proc.* 41, 685–691. <https://doi.org/10.1016/j.matpr.2020.05.435>.
- Ullah, A., Yin, X., Wang, F., Xu, B.O., Mirani, Z.A., Xu, B., Chan, M.W.H., Ali, A., Usman, M., Ali, N., Naveed, M., 2021. Biosynthesis of selenium nanoparticles (via *Bacillus subtilis* BSN313), and their isolation, characterization, and bioactivities. *Molecules* 26, <https://doi.org/10.3390/molecules26185559> 5559.
- Upadhyay, P.K., Jain, V.K., Sharma, S., Shrivastav, A.K., Sharma, R., 2020. Green and chemically synthesized ZnO nanoparticles: A comparative study. *IOP Conf. Ser. Mater. Sci. Eng.* 798, <https://doi.org/10.1088/1757-899X/798/1/012025> 012025.
- Vasconcelos, N.G., Croda, J., Simionatto, S., 2018. Antibacterial mechanisms of cinnamon and its constituents: A review. *Microb. Pathog.* 120, 198–203. <https://doi.org/10.1016/j.micpath.2018.04.036>.

- Vijayaraghavan, P., Arun, A., Al-Dhabi, N.A., Vincent, S.G.P., Arasu, M.V., Choi, K.C., 2016. Novel *Bacillus subtilis* IND19 cell factory for the simultaneous production of carboxy methyl cellulase and protease using cow dung substrate in solid-substrate fermentation. *Biotechnol. Biofuels* 9., <https://doi.org/10.1186/s13068-016-0481-6> 73.
- Wehaidy, H.R., Abdel Wahab, W.A., Kholif, A.M.M., Elaaser, M., Bahgaat, W.K., Abdel-Naby, M.A., 2020. Statistical optimization of *B. subtilis* MK775302 milk clotting enzyme production using agro-industrial residues, enzyme characterization and application in cheese manufacture. *Biocatal. Agric. Biotechnol.* 25., <https://doi.org/10.1016/j.bcab.2020.101589> 101589.
- Yildirim, V., Baltaci, M.O., Ozgencli, I., Sisecioglu, M., Adiguzel, A., Adiguzel, G., 2017. Purification and biochemical characterization of a novel thermostable serine alkaline protease from *Aeribacillus pallidus* C10: a potential additive for detergents. *J. Enzyme Inhib. Med. Chem.* 32, 468–477. <https://doi.org/10.1080/14756366.2016.1261131>.
- Yu, X., Li, J., Mu, D., Zhang, H., Liu, Q., Chen, G., 2021. Green synthesis and characterizations of silver nanoparticles with enhanced antibacterial properties by secondary metabolites of *Bacillus subtilis* (SDUM301120). *Green Chem. Lett. Rev.* 14, 190–203. <https://doi.org/10.1080/17518253.2021.1894244>.
- Zhou, J., Liu, Y., Shen, T., Chen, L., Zhang, C., Cai, K., Liao, C., Wang, C., 2019. Antimicrobial activity of the antibacterial peptide PMAP-36 and its analogues. *Microb. Pathog.* 136., <https://doi.org/10.1016/j.micpath.2019.103712> 103712.